International Journal of Architectural Heritage
Conservation, Analysis, and Restoration

ISSN: 1558-3058 (Print) 1558-3066 (Online) Journal homepage: https://www.tandfonline.com/loi/uarc20

Seismic Vulnerability of Historical Masonry Aggregate Buildings in Oriental Sicily

A. Greco, G. Lombardo, B. Pantò & A. Famà

To cite this article: A. Greco, G. Lombardo, B. Pantò & A. Famà (2020) Seismic Vulnerability of Historical Masonry Aggregate Buildings in Oriental Sicily, International Journal of Architectural Heritage, 14:4, 517-540, DOI: 10.1080/15583058.2018.1553075

To link to this article: https://doi.org/10.1080/15583058.2018.1553075

INTERNATIONAL JOURNAL OF ARCHITECTURAL HERITAGE
2020, VOL. 14, NO. 4, 517–540
https://doi.org/10.1080/15583058.2018.1553075

Taylor & Francis
Taylor & Francis Group

Seismic Vulnerability of Historical Masonry Aggregate Buildings in Oriental Sicily

A. Greco, G. Lombardo, B. Pantò, and A. Famà

Department of Civil Engineering and Architecture, University of Catania, Catania, Italy

ABSTRACT

The seismic vulnerability assessment of historical UnReinforced Masonry (URM) buildings is a very complex task since it is strongly related to a great variety both of geometrical layouts and of masonry mechanical characteristics. In this article, some results of a Catania University research project, denomined "FIR 2014", focused on the seismic vulnerability estimation of historical buildings, built in Catania after the 1963 earthquake, are presented. First, a detailed typological analysis of the considered urban fabric, characterized by typical residential masonry buildings, has been performed. Such analysis allowed recognizing an elementary structural modulus, which has been studied according to different geometrical layouts representative of isolated or aggregate buildings. The results of nonlinear static analyses, performed by applying an innovative macro-element approach, allowed for the assessment the seismic vulnerability of typical URM buildings coherently to the Italian seismic code. The adopted macro-element strategy for the seismic assessment of aggregate masonry buildings, although related to a specific historical center, may be applied to similar urban fabrics and can also be used for the calibration and validation of fast seismic assessment strategies, particularly useful for the evaluation of the seismic risk at urban scale.

ARTICLE HISTORY
Received 23 July 2018
Accepted 22 November 2018

KEYWORDS
Cultural heritage preservation; historical aggregate buildings; masonry buildings; macro-modeling approach; push-over analyses; Seismic vulnerability

1. Introduction

Seismic vulnerability assessments can be performed at different scales, from a single building to large urban areas. The seismic vulnerability evaluation on a single building has to provide detailed information on the susceptibility of the structure to suffer damage during the expected seismic events in the construction site. The urban vulnerability, more generally, is related to the individual vulnerabilities of buildings in a larger context that can represent a whole city or a significant portion of it (Giuffre 1993; Ferreira et al. 2013; Maio et al. 2016; Maio, Ferreira, and Vicente 2016). It turns out that, in general, the change in scale involves a reduction in the accuracy of the results due to the amount of data and resources involved in a rigorous assessment (Ramos and Lourenço 2004; Mallardo et al. 2008; Pujades et al. 2012; Maio et al. 2015; Formisano 2017; Fagundes, Bento, and Cattari 2017).

In fact, the analysis of the vulnerability of a single building requires the detailed knowledge of its geometry and of the mechanical properties of its construction materials, and therefore presents some limits associated with the need of conducting in situ structural tests. (Betti, Bartoli, and Orlando 2010; Andreini et al. 2013a, 2013b; Casapulla, Argiento, and Maione 2017a, 2017b). This information is preparatory to the evaluation of the seismic performance of the building obtained through complex numerical simulations (Caddemi et al. 2014; Pantò et al. 2016; Cannizzaro et al. 2017; Fortunato et al. 2017), also in the of retrofitting strategies like FRP (Bertolesi et al. 201 7; Ramaglia et al. 2018) or FRCM (D'Ambra et al. 2018) reinforcement systems. Due to the computational cost and to the implementation time related to a detailed analysis it is nowadays unsustainable to extend the same approach to a large urban context or to large aggregate of buildings.

On the other hand, the knowledge of the seismic response of individual buildings of an aggregate is not sufficient to explain some typical aspects of the behavior of overall aggregate such as, for example, the interaction between adjacent buildings or the activation of partial collapses. Furthermore, the seismic response of aggregates of masonry buildings is often influenced by the presence of weak and deformable floor diaphragms and irregular layouts which lead to complex dynamic actions involving in-plane and out-of-plane behavior of each structural unit (Paquette and Bruneau 2006; Lourenço et al. 2011; Betti, Galano, and Vignoli 2014). For the above reasons, a detailed

CONTACT Bartolomeo Pantò bpanto@dica.unict.it Department of Civil Engineering and Architecture,University of Catania, viale A. Doria 6, Catania, Italy
Color versions of one or more of the figures in the article can be found online at www.tandfonline.com/uarc.

numerical simulation of the aggregate seismic response requires nonlinear dynamic analyses (Senaldi, Magenes, and Penna 2010; Chácara et al., 2018) which, however, due to their high computational burden, are unsuitable to be applied by practitioners. Pushover analyses, even though approximated, can represent an applicable tool for the investigation of the nonlinear global behavior of both isolated and aggregate structures and the assessment of their seismic safety factors (Marques, Vasconcelos, and Lourenço 2012; Cannizzaro et al. 2017).

The purpose of the present research is to provide simplified, but at the same time sufficiently accurate, numerical methodologies for the evaluation of the seismic vulnerability of historical urban centres. The approach here adopted is conceived with the aim of extending the results obtained for some identifiable typologies of single buildings to more complex structural layouts. The article reports some results of the application of the proposed strategy to the analysis and evaluation of the seismic vulnerability of some areas of the historic centre of Catania, in Sicily, built after the strong earthquake of 1693.

The first needed step is based on a broad recognition of building typologies recurrent in the considered areas (Cicero and Lombardo 2015). The analyzed urban fabric is mainly constituted of residential buildings belonging to citizen of the lower/middle class. By means of historic data, and where possible direct inspections, it has been possible to recognize the diffused presence of an elementary modulus, denoted as "cell" in the following, that can either represent a single building or can be assembled to form different "structural units" (SU). The latter have been classified in some typical structural typologies (archetype) representative of the considered urban historical fabric. Each archetype represents a wide class of similar historical masonry buildings possessing strong similarities in terms of geometrical layout, construction methodologies and material properties (Barbera 1992). In order to obtain a structural model of each archetype, the mechanical characteristics of the masonry have been selected considering material parameters representative of the constructions built in Catania between the 18th and 20th century. In the present study, both the geometrical and mechanical characteristics of each structural unit have been assumed as deterministic values; successive developments could involve probability distributions of the required data.

For each structural unit and aggregate of units, knowing the geometrical structural layout and the material properties, three-dimensional numerical models have been defined by means of an innovative macro-modeling strategy based on a 2D macro-model proposed by a research team of the University of Catania (Caliò, Marletta, and Pantò 2012). This strategy has allowed to perform the numerical analyses with a reduced computational effort compared to that required by advanced finite element models. Namely, the three-dimensional models have been implemented in the structural code 3DMacro (Gruppo Sismica srl 2012) currently employed for academic research and engineering practice either to estimate the seismic vulnerability of existing unreinforced (Marques and Lourenço 2011) and mixed masonry structures (Andreini et al. 2014; Caliò et al. 2008), or for seismic design of new confined and unconfined masonry buildings (Marques and Lourenço 2014). Besides analyzing the seismic response of each individual structural unit, its role within the aggregate has been analysed with the aim to highlight the different behavior of the unit when considered as isolated or part of an aggregate. The results of the pushover curves have been analyzed considering the procedure suggested by the Italian building code (NTC 2018) providing a code-consistent seismic vulnerability assessment and the corresponding vulnerability index for all the investigated cases.

The proposed approach and the obtained results, although related to typical Catania's historical fabric, could also be extended to other urban centres having similar characteristics and used for the evaluation of seismic risk at urban scale.

2. Typological analysis of the buildings of the historic center of Catania

In this section some typical geometrical layouts and masonry mechanical characteristics of historical residential buildings built in Catania in the 19th century are considered with the aim to identify groups of buildings according to their shared morphological and constructive characteristics (Barbera 1992). A common element in all the considered cases is that the constructive system of the masonry walls is characterized by the presence of regular or irregular volcanic stones with different mechanical parameters (Barbera 1992). The simplest residential unit that has been identified is associated to a mono-cellular type. The basic identified cell has a regular plan with dimensions 5.5 m x 6.5 m and height 4.5 m; the door openings are 1.2 x 3.0 m. Balconies have a length of 0.6 m and a total width, symmetrical to the opening, of 2.5 m. Different combinations of the basic cell are then considered leading to more complex geometrical layouts representative of several historical buildings in Catania. In the generation process from the single cell to the assembled structure,

identifying the aggregate, it has been assumed that the structural connections between the cells are strong enough to allow the aggregate to be considered as a single structure. According to the performed survey, nine typological classes have been identified as reported in the following.

A-single-story house: representing the simplest identified structural unit, is characterized by the presence of one (*A1*, Monocellular, Figure 1) or two cells (*A2*, Bicellular, Figure 2)

B-Terraced house: a multi-story building whose main front has the width of one cell and, in the orthogonal direction, can be composed by one (*B1*, Monocellular, Figure 3) or two cells (*B2*, Bicellular, Figure 4). In the typology *B1* the building has three floors while in *B2* the floors are two.

C-Block of flats: a building with three floors whose main front is composed by two (*C2*, Bicellular, Figure 5), three (*C3*, Tricellular, Figure 6), or four cells (*C4*, Quadricellular, Figure 7) while in the orthogonal direction is composed by two cells.

D-Patio house: large building with three floors whose main front has the width of five cells while in the orthogonal direction is composed by four cells. They are characterized by the presence of a patio that can be situated on one side (*DA*, Open Patio, Figure 8) or in the middle (*DC*, Closed Patio, Figures 9) of the building.

In order to identify the presence of these typological classes in the considered urban fabric, in the following they will be characterized by different colours, in particular: *A* = orange, *B* = blue, *C* = red, *D* = green. Figures 1–9 show, for each typological class, the plan views and the façades together with a picture of a real example in the considered urban area.

The above-described structural typologies are frequent in the historic residential fabric in Catania either as isolated buildings or as aggregates (Giuffrè 1993). Figure 10 shows three examples of aggregates of buildings in which the identified typologies can be easily recognized.

3. Mechanical characterization of the masonry

The mechanical performance of historical masonry walls is strongly influenced by the properties of their components (stones or bricks and mortar) and their

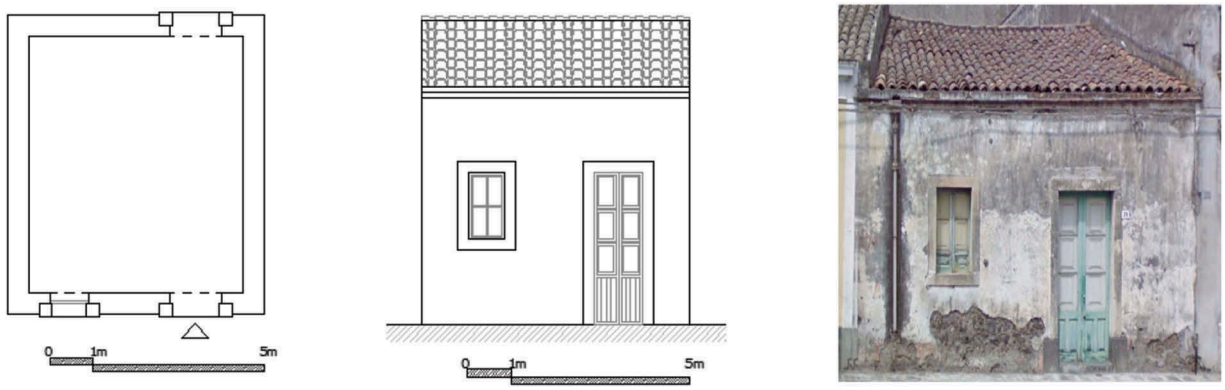

Figure 1. Monocellular Single-Story House (**A1**), from the left: plan, façade, real example.

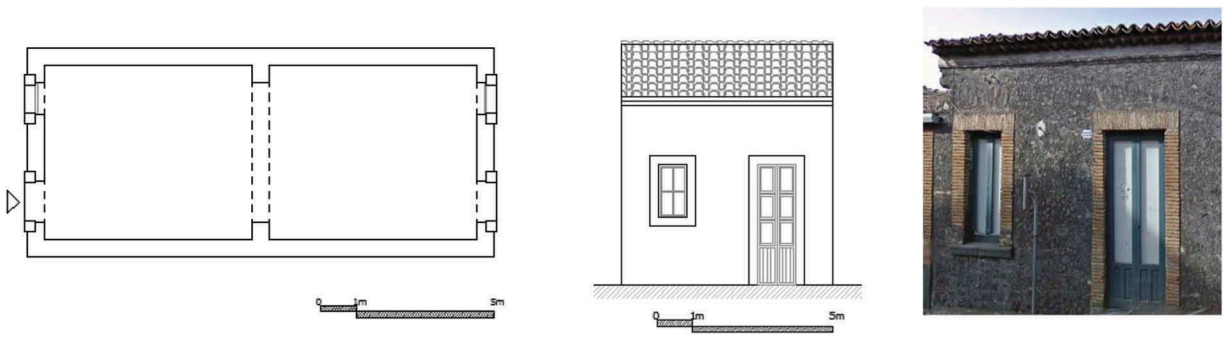

Figure 2. Bicellular Single-Story House (**A2**), from the left: plan, façade, real example.

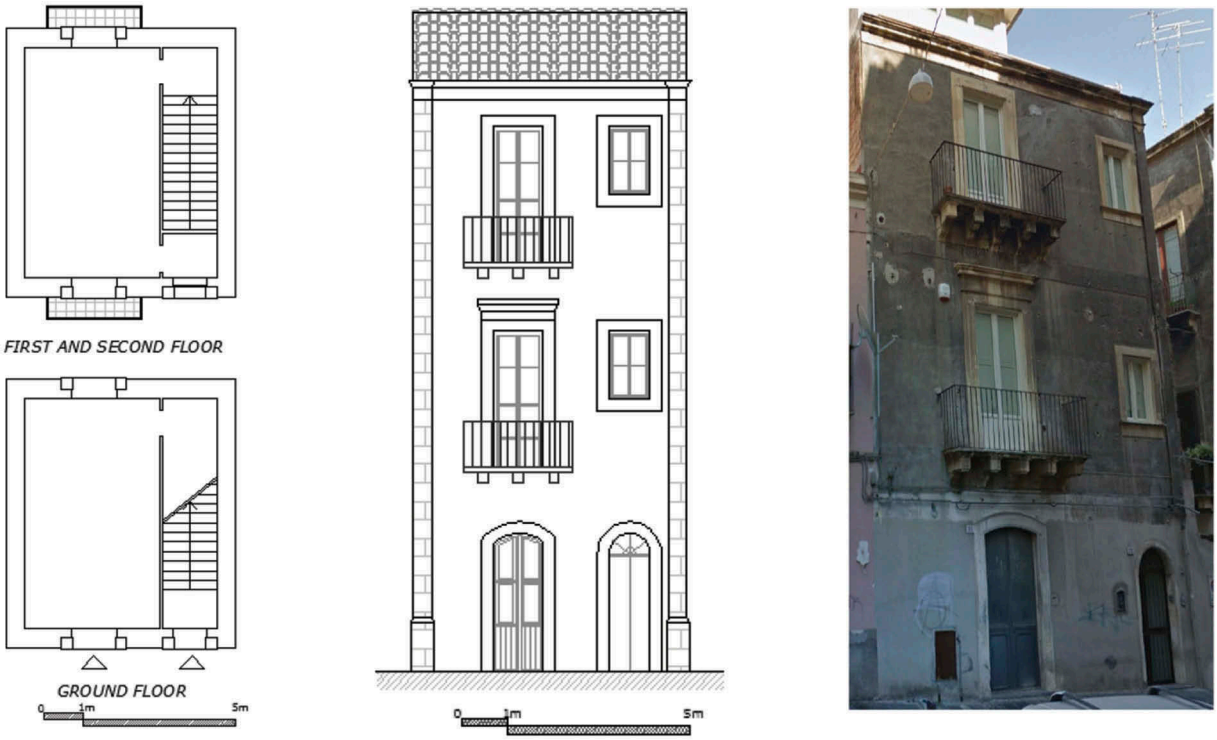

Figure 3. Monocellular Terraced House (**B1**), from the left: plan, façade, real example.

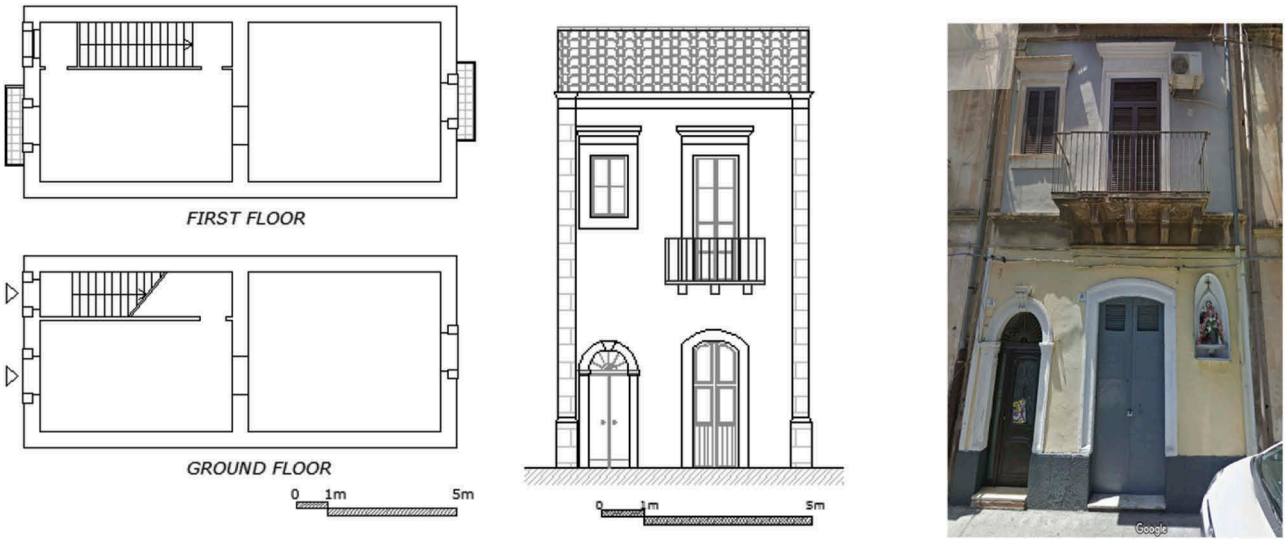

Figure 4. Bicellular Terraced House (**B2**), from the left: plan, façade, real example.

arrangement within the walls (Borri et al. 2015). Both of these aspects play a fundamental role in the determination of the stiffness, strength, and ductility of masonry walls against horizontal seismic actions. In particular, the quality of the transversal masonry arrangement influences the capability of the panels of exhibiting an almost monolithic behavior under cyclic out-of-plane loads avoiding phenomena of desegregation. Therefore, since historical masonry structures present a high variability in terms of mechanical characteristics, specific tests, and survey inspections are necessary to evaluate the input constitutive parameters in order to perform nonlinear numerical simulations.

In the historical constructive practice in the area of Catania, volcanic stones extracted from the lava flow of the nearby Etna volcano have been largely used to build masonry walls, arches and vaults. This material is

Figure 5. Bicellular Block of Flats (**C2**), from the left: plan, façade, real example.

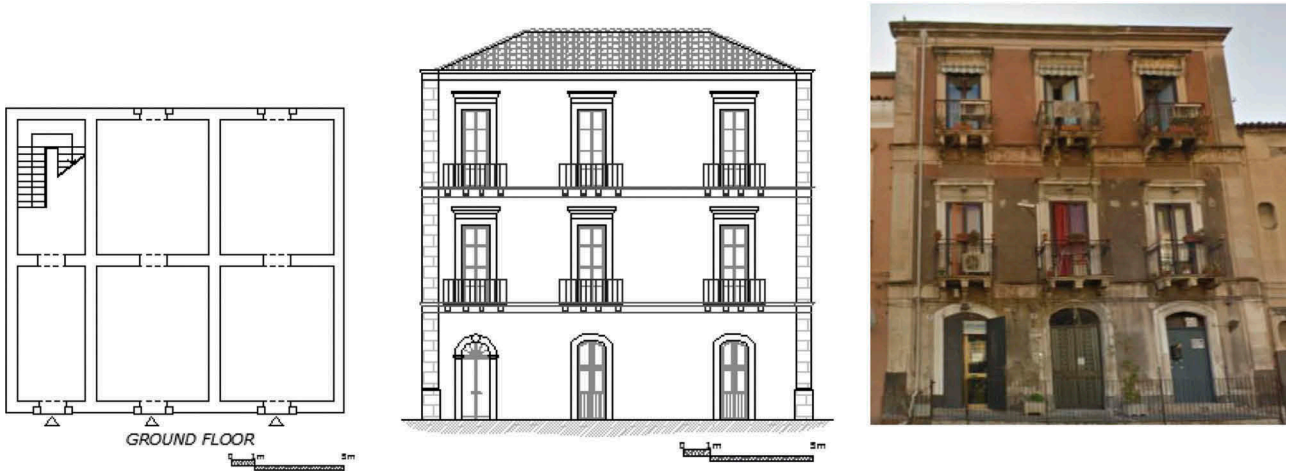

Figure 6. Tricellular Block of Flats (**C3**), from the left: plan, façade, real example.

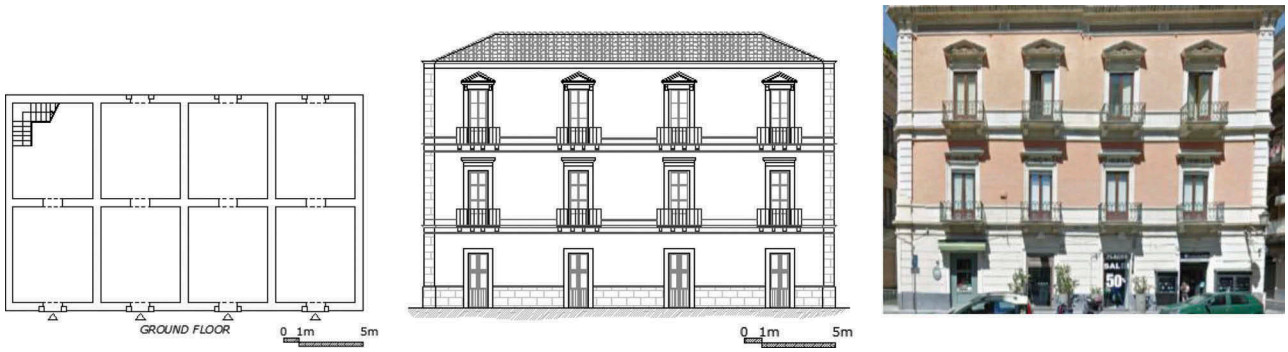

Figure 7. Quadricellular Block of Flats (**C4**), from the left: plan, façade, real example.

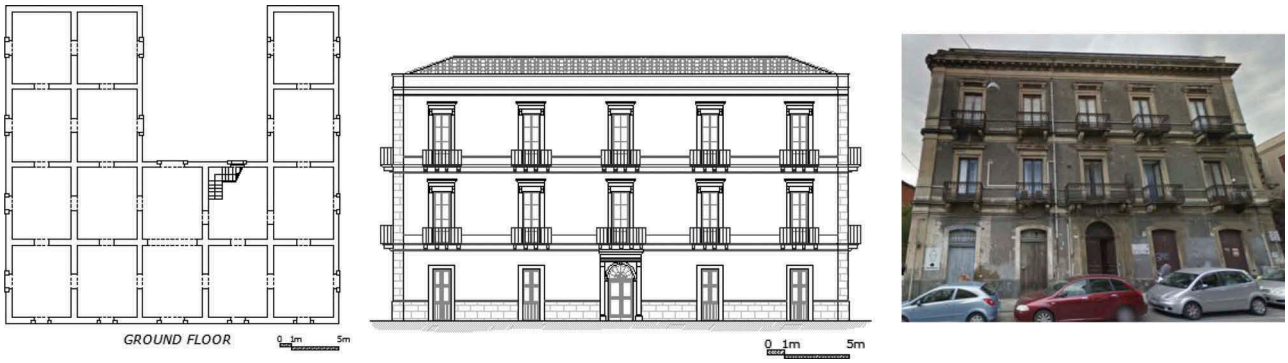

Figure 8. Open Patio House (**DA**), from the left: plan, façade, real example.

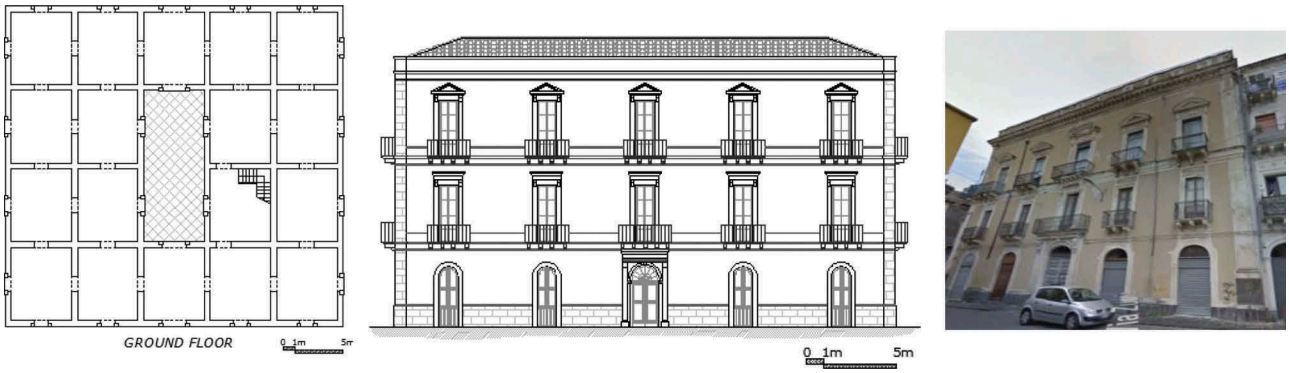

Figure 9. Closed Patio House (**DC**), from the left: plan, façade, real example.

characterized by a high mechanical resistance and elastic modulus and presents a good workability (Anania, Badala, and Cuomo 1995). This material has been used in a wide range of shapes and sizes: irregular stones, elements roughly squared only in the external face, and squared blocks. Since the compressive strength of these units is generally higher than 100 MPa, the structural collapse is rarely associated to the rupture of the stones. However, a mortar with low mechanical properties was generally used and therefore the in-plane structural failure is potentially associated to tensile cracking or sliding at the mortar joints. The masonry panels are generally characterized by a limited ductility capacity, as verified by means of experimental tests (Anania, Badala, and Cuomo 1995) and in situ tests performed on numerous masonry arrangements (Caliò 2011; Andreini et al. 2013a).

The mechanical parameters, used in the analyses reported in the following, are based on the results of non-destructive or low-destructive in situ tests performed on masonry typologies representative of the historical constructions built in the area of Catania between the 18th and the early 20th century (Beolchi et al. 2000; Binda 2000). In particular, reference is made to the normal and tangential moduli of deformation, the compressive and shear strengths. An exhaustive description of the macroscopic and mechanical characteristics of the most diffused masonry typologies in the area of interest, is reported in Beolchi et al. (2000) while in Binda (2000) the survey techniques and in-situ tests, suitable to characterize the masonry, are described and discussed.

In the analyses reported in the following sections, two stone masonry typologies, representative of the tradition of construction for residential buildings in Catania during the 19th century, are considered. These are classified as a *medium quality masonry* (Figure 11a) characterized by square stones with a good arrangement and presence of transversal connections within the walls thickness, and a *poor quality masonry* (Figure 11b) characterized by an irregular disposition of smaller stones. In the latter case, the wall is composed by a double leaf with few transversal connections.

The mechanical parameters used in the numerical analyses, summarized in Table 1, are evaluated coherently to the data provided in the literature and comply with the requirements of the Italian code. In the table, E and G are the normal and tangential moduli of

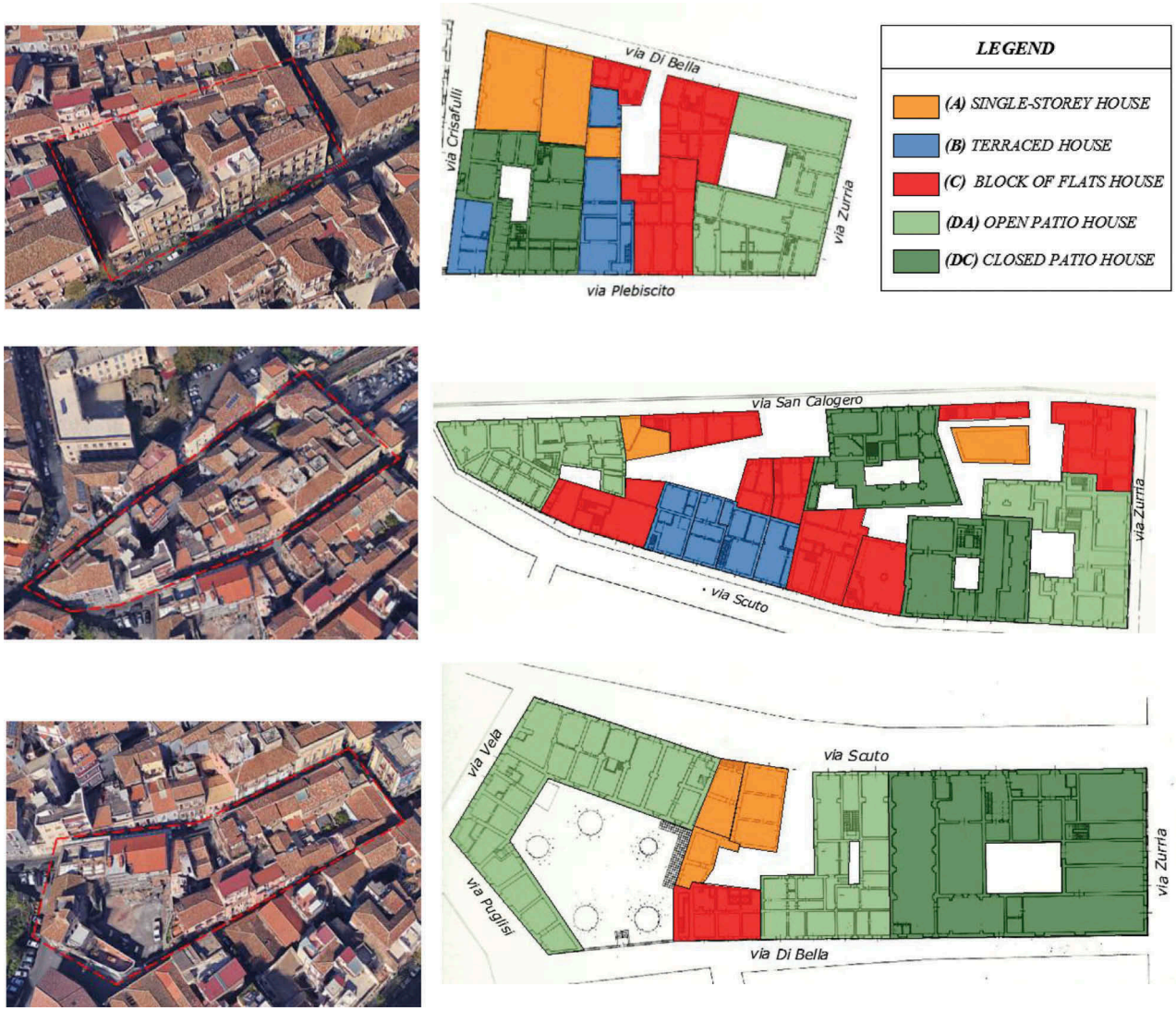

Figure 10. Some examples of structural aggregates.

deformation, f_m and f_{tm} are the compressive and tensile strengths, Γ_o is the average tangential stress in the shear force direction associated to the diagonal shear failure in absence of axial force, and w is the specific weight.

In the performed analyses the flexural behavior of the masonry has been considered as elasto-perfectly plastic with limited ductility. The strength in tension is conventionally assumed 1/20 of the compressive strength and limited ductility capacities of 1.5 are considered both in tension and compression. An elasto-plastic constitutive law, governed by the Tusnsek and Cacovic criteria (Tusnsek and Cacovic 1971) is considered for simulating the shear diagonal failure mechanism. According to the Italian code prescriptions and the experimental data available for similar masonry typologies, ultimate drifts of 0.4% and 0.6% are assumed respectively for shear and flexural failure.

4. Seismic vulnerability assessment of the considered case studies

In this section, the seismic vulnerability assessment of the structural typologies identified in the previous section is presented. The nonlinear structural analyses are performed according to an original numerical modeling strategy, based on the use of a 2D macro-element, capable of analysing the collapse behavior of unreinforced (Caliò, Marletta, and Pantò 2012) and confined (Caliò and Pantò 2014) masonry buildings with a reduced computational effort if compared to the rigorous, although computational expensive, nonlinear finite element approaches. The strategy has been experimentally validated (Pantò et al. 2017a, 2017b Pantò, 2017b) and numerically compared to other simplified approaches proposed in the literature (Pantò

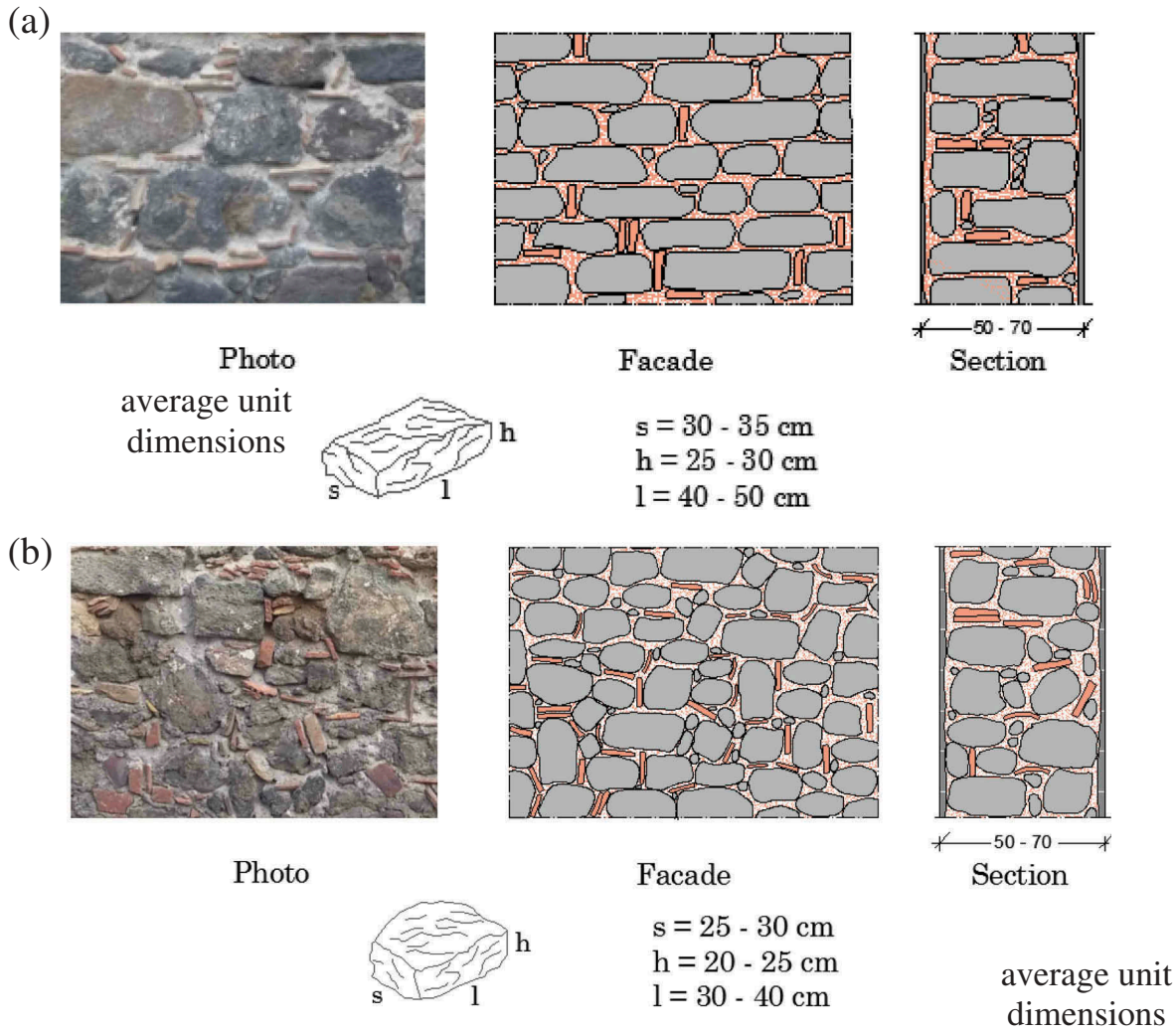

Figure 11. Masonry typologies: Medium quality of masonry (a); poor quality of masonry (b).

Table 1. Mechanical parameters of the masonry considered in the analyses.

Masonry typologies	E (Mpa)	G (Mpa)	W (kN/m^3)	f_m (kN/m^2)	f_{tm} (kN/m^2)	τ_0 (kN/m^2)
medium quality	4000	1600	22	3,0	0,050	0,043
poor quality	2000	800	22	2,0	0,033	0,027

et al. 2015). This 2D macro-model can be represented by an equivalent mechanical scheme constituted by an articulated quadrilateral with rigid edges, connected by four hinges and two nonlinear diagonal links that simulate the diagonal shear failure of a masonry macro-portion. Along each side, the quadrilateral interacts with the contiguous panels by means of interfaces simulating the axial-flexural behavior of masonry as well as the potential sliding along the mortar joints. Each masonry wall can be obtained by a basic mesh (each quadrilateral represents a masonry pier or spandrel) or refined mesh of macro-elements, according to the opening dispositions (Caliò, Marletta, and Pantò 2012). The model calibration is performed enforcing equivalence between the masonry media and a reference continuous model following a *fiber calibration procedure*, based only on the panel geometry and on the main mechanical parameters macroscopically characterising the masonry. The models of the considered structural typologies have been implemented in the computer code 3DMacro (Gruppo Sismica 2012).

The numerical simulations and the seismic vulnerability factors are obtained under the assumption that the out-of-plane failure of the masonry walls is prevented due to either the presence of efficient

connections between orthogonal walls or the insertion of tie rods. As a result, a box-behavior of each considered structure with respect to seismic actions is considered in accordance with current technical standards.

Four typologies of floors are considered in the models according to the practice typically used in the reference period of construction. These are shown in Figure 12: a barrel vault at the first level (Figure 12a), mixed steel-masonry and steel-concrete horizontal slabs at the upper intermediate floors (Figure 12b–c) and an inclined wooden diaphragm at the roof level (Figure 12d). The first diaphragm typology considered for the intermediate levels is constituted by steel beams supporting brick masonry vaults, covered by incoherent material or unreinforced concrete in order to obtain an horizontal extrados (Figure 12b); in the second typology, the steel beams support hollowed flat bricks covered with unreinforced concrete (Figure 12c).

In the numerical analyses, all the diaphragms are modelled by means of an equivalent elastic orthotropic membrane with appropriate thickness. The characteristic parameters of the equivalent membrane are summarized in Table 2 where for each typology the thickness (t_e), the longitudinal (E_{long}) and transversal (E_{transv}) elasticity moduli, and the tangential deformation modulus (G) are indicated. With reference to the masonry vaults, the equivalent diaphragm parameters are evaluated according to the procedures proposed in (Cattari, Resemini, and Lagomarsino 2008; Marseglia et al. 2014; Giresini et al. 2017) considering a constant average thickness of the vault equal to 30 cm. The elastic deformability of the flat slabs are evaluated according to (NZSEE 2015) considering weak diaphragm-to wall connections. The last two columns of Table 2 report the structural and non-structural permanent loads (Q_{dead}) and the variable loads (Q_{live}) uniformly applied to the models, before the seismic analyses.

In the following analyses reference will be made to seismic loads in the direction parallel to the main facade of each building (X direction) and in the orthogonal one (Y direction).

First, a modal characterization of each structural unit has been carried out by performing modal analyses. The results are reported in Table 3 where the fundamental periods in the X direction (T_x) and in the orthogonal one (T_y) are reported with the corresponding effective masses ($M_{eff,x}$ and $M_{eff,y}$) expressed as a percentage of the total mass of the building. It is

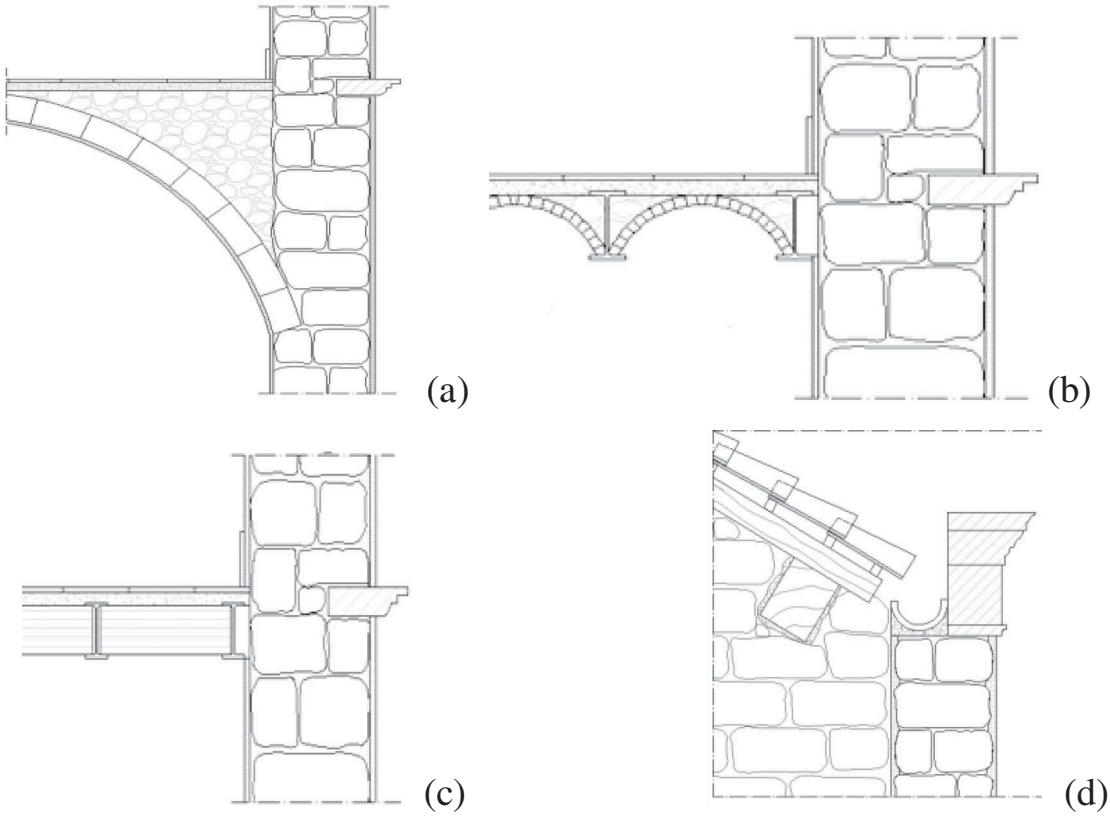

Figure 12. Diaphragm typologies: barrel vault (a); mixed steel-masonry horizontal diaphragm (b); mixed steel-concrete horizontal diaphragm (c); inclined wooden top cover floor (d).

Table 2. Equivalent orthotropic membrane simulating the diaphragms and the gravity loads.

Floors typology	t_e (cm)	E_{long} (Mpa)	E_{transv} (Mpa)	G (Mpa)	Q_{dead} (KN/m^2)	Q_{live} (KN/m)
barrel vault	20	3000	2000	1000	8.00	2.00
mixed horizontal steel-masonry	4	2500	1250	650	3.00	2.00
wooden top floor	2	1500	750	300	1.50	0.50

important to notice that for each building typology the fundamental modes activate a considerable amount of mass. In most cases, the mass involved ranged between 50% and 75% of the total seismic mass of the building. Lower effective masses are observed in the *Y* direction both in the case of *DA* typology (33%) due to its in-plane irregularity and the *A-B* typologies (up to 35%) due to the floor-diaphragms deformability.

The evaluation of the seismic vulnerability of the structure is performed in the nonlinear field through incremental nonlinear static analyses, consistent to the Italian seismic code (NTC 2018, Italian Ministry of Infrastructure, D.M 2018), assuming mass-proportional force distributions. Due to the small heights of all the investigated buildings this load distribution can be considered a good representation of the actual distribution of the inertia forces. The results of the analyses are reported in the following section in terms of capacity curves and collapse mechanisms. Subsequently, the seismic vulnerability of each structural typology is expressed in terms of admissible Peak Ground Acceleration (*PGA*) guaranteeing equal seismic demand and displacement capacity. In the numerical simulations reference is made to both the two conditions of poor- and medium-quality masonry described in the previous section.

4.1. Seismic behavior of the structural units

In this section, the seismic behavior of each structural typology considered as an isolated building, is investigated. The aim of this preliminary study is to provide a characterization of the structural typologies in order to get a deep understanding of their interaction when they belong to an aggregate. The interaction between the orthogonal walls, as well as the out-of-plane contribution of the walls, are neglected in the simulations.

Table 3. Modal characterization of the isolated structural typologies.

Typology	T_x (sec)	T_y (sec)	$M_{eff,x}$ (%)	$M_{eff,y}$ (%)
A1	0.182	0.228	45.66	32.72
A2	0.149	0.239	31.80	61.00
B1	0.254	0.392	65.93	76.08
B2	0.296	0.172	72.44	22.66
C2	0.200	0.269	50.81	72.62
C3	0.240	0.196	73.51	55.91
C4	0.193	0.184	54.11	68.14
DA	0.190	0.230	62.50	33.32
DC	0.184	0.231	72.13	63.76

The results are presented in terms of capacity curves plotting the base shear coefficient (C_b), defined as the ratio between the base shear of the structure (V_b) and its seismic weight (W), as a function of the top displacement of each building. The seismic weight of each building corresponds to the structural weights (masonry and slabs) plus the permanent and variable loads applied at the floor levels, combined according to NTC2018.

The solutions for the incremental steps are obtained through the Newton-Raphson method combined with an arc-length technique to allow the simulation of the softening branch. The evaluation of the post-peak response is required for providing a seismic vulnerability assessment consistent to the Italian building code.

Figures 13–14 report the capacity curves in the *X* and *Y* direction, respectively. With reference to the *X* direction, the maximum shear coefficients of the buildings range approximately from 5–12% of the corresponding seismic weight. The weakest strengths are associated to the typologies *B* and *C*, depending on the number of cells and levels, while the highest strengths are associated to the typology *A*. Increasing the number of cells, in comparison to the monocellular typology, an increase of the values of the lateral stiffness and strength is observed. Typologies *B* and *C* are characterized by a ductile response while *A* and *D* present a more brittle post-peak behavior with a gradual softening in the case of typology *D*, and a drop of resistance in the case of *A*.

The analyses in the *Y* direction show lateral strengths higher than those in the *X* direction; the minimum base shear coefficient is approximately 0.15 and is associated to the typology *D* while, the maximum value, associated to the typology *A*, is 0.45. Most of the investigated typologies show a good displacement capacity with the exception of *A1, A2*, and *B2* in which the ultimate displacement, correspondent to a drastic drop of resistance, is smaller than 2 cm. Moreover, the analyses of typology *C4* halted at approximately 1.5 cm due to the occurrence of local structural collapses.

The comparison of the response in the two directions shows how the opening distribution causes a high reduction of the building resistances measured in terms

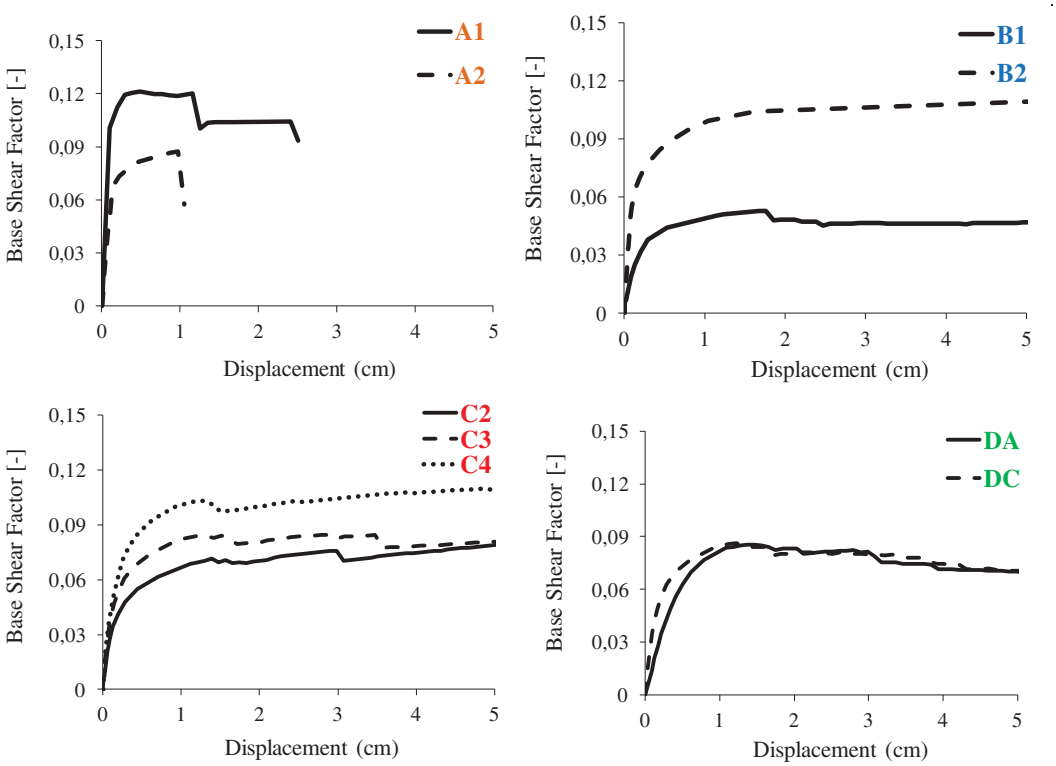

Figure 13. Capacity curves of the building typologies in the direction X.

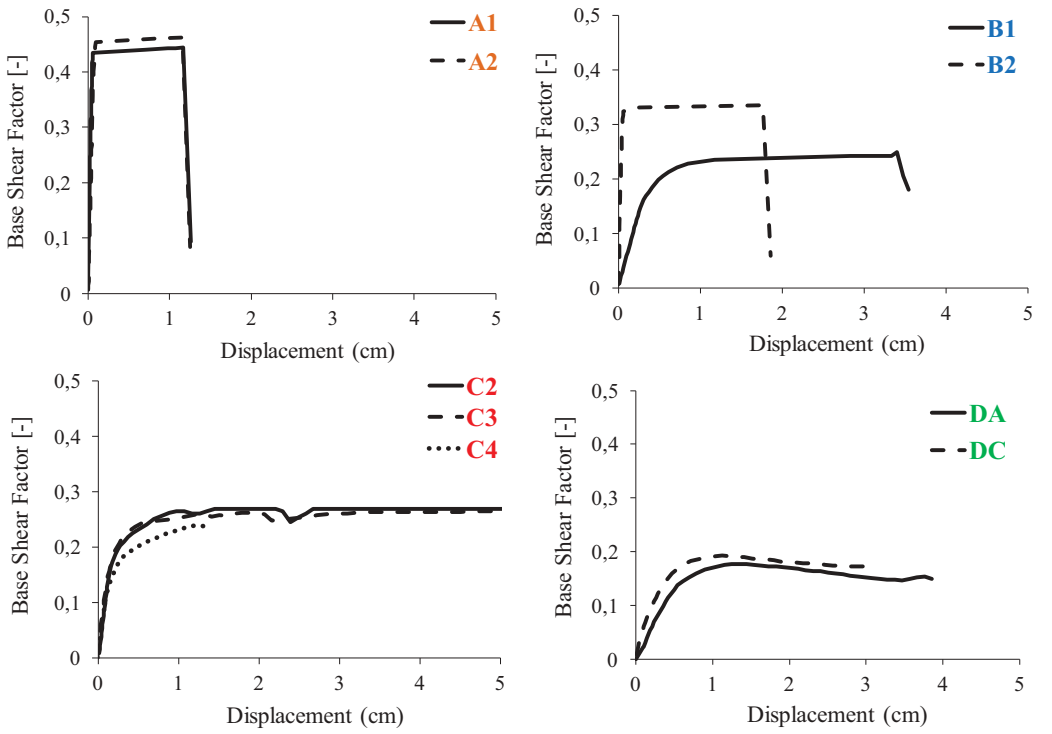

Figure 14. Capacity curves of the building typologies in the *Y* direction .

of the peak value of C_b. The differences between the responses in the two directions are also due to the different geometry and effective masonry area present in each direction.

The collapse mechanisms and the corresponding damage patterns are shown in Figures 15–16 with reference to the *C2* and *DA* typologies, respectively. It can be observed that the damage is mostly

concentrated in the spandrels, characterized by a diagonal shear mechanism, while the masonry piers show a rocking mechanism. These are typical failure modes in the absence of rigid floors and floor beams. It is worth noticing that the predicted damage scenario are consistent to what has been observed after real seismic events, such as the 2009 L'Aquila earthquake (Indirli et al. 2013) and 2016 Centre Italy earthquakes (Fiorentino et al. 2018) in similar historical buildings.

In Figures 17–18, considering both load directions *X* and *Y*, the influence of the mechanical quality of the masonry on the capacity curves is shown with reference to the typologies *C2* and *DA*. A limited influence of the masonry quality on the structural response is observed in terms of maximum base shear and ductility capacity. However, the analyses obtained considering a poor-quality masonry showed a significant reduction in the initial lateral stiffness and a different nonlinear behavior.

The direction *Y* is more influenced than *X* by the masonry changes both in terms of stiffness and strength variations. The highest differences in terms of base shear are registered in the analyses regarding the typology *DA* (Figure 18a–b).

4.2. Assessment of the seismic safety indices of the isolated structural units

In this section, the pushover curves, presented in Section 4.1, are used to perform the seismic assessment according to the N2 method (Fajfar and Gaspersic 1996) and to the prescriptions reported in the Italian code (NTC 2018, Italian Ministry of Infrastructure, D.M 2018). With this aim, the collapse limit state, related to a reduction of 20% of the global base shear, is considered. An equivalent single degree of freedom (*SDOF*) system is obtained from the bi-linearized equivalent capacity curves of the MDOF system, dividing the base shear force (V_b) and the displacement of the target point by the modal participation factor (Γ). The latter factor is calculated taking into account the masses and the fundamental modal shape in the considered

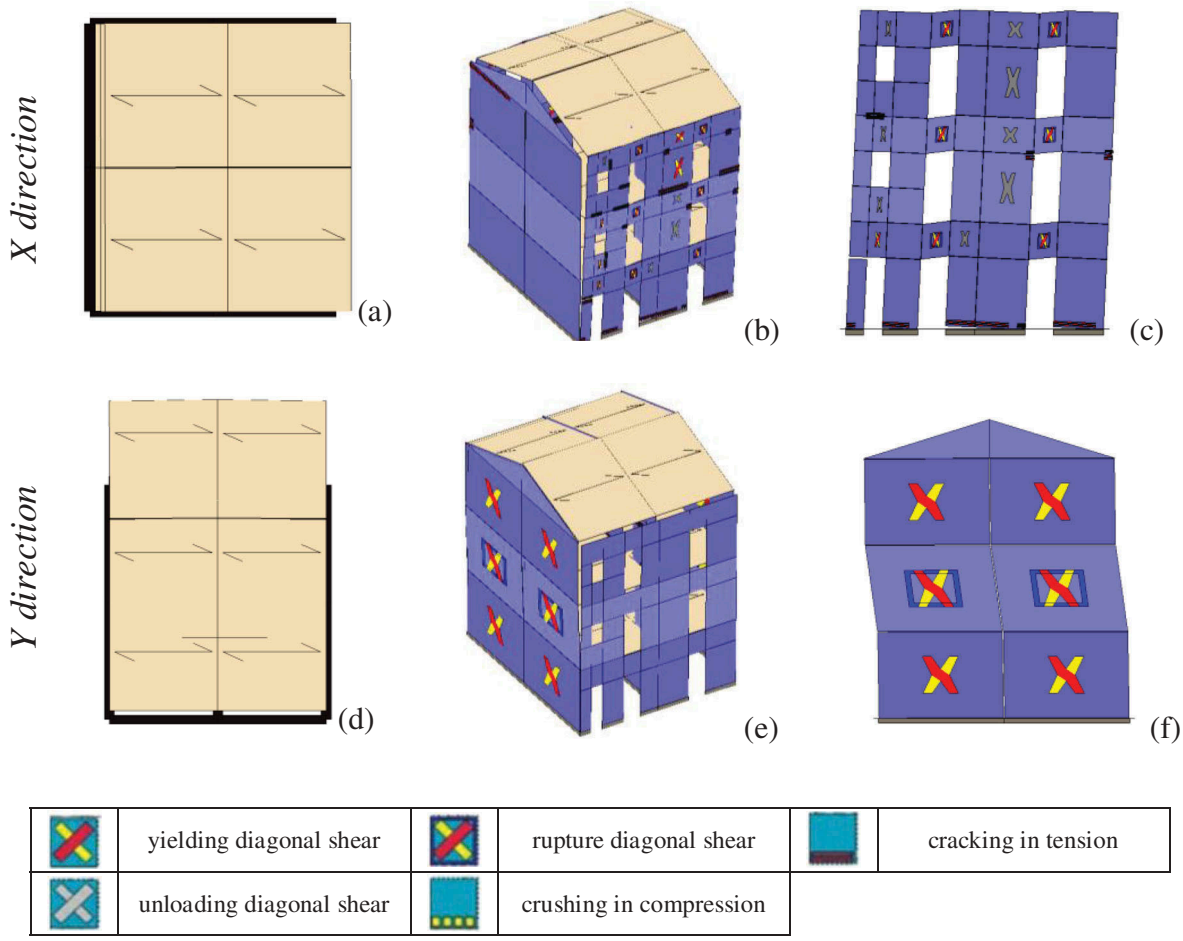

Figure 15. Collapse mechanisms of the **C2** model loaded in the *X* and *Y* directions: Plan view (a, d); 3D view (b, e); main facade (c, f).

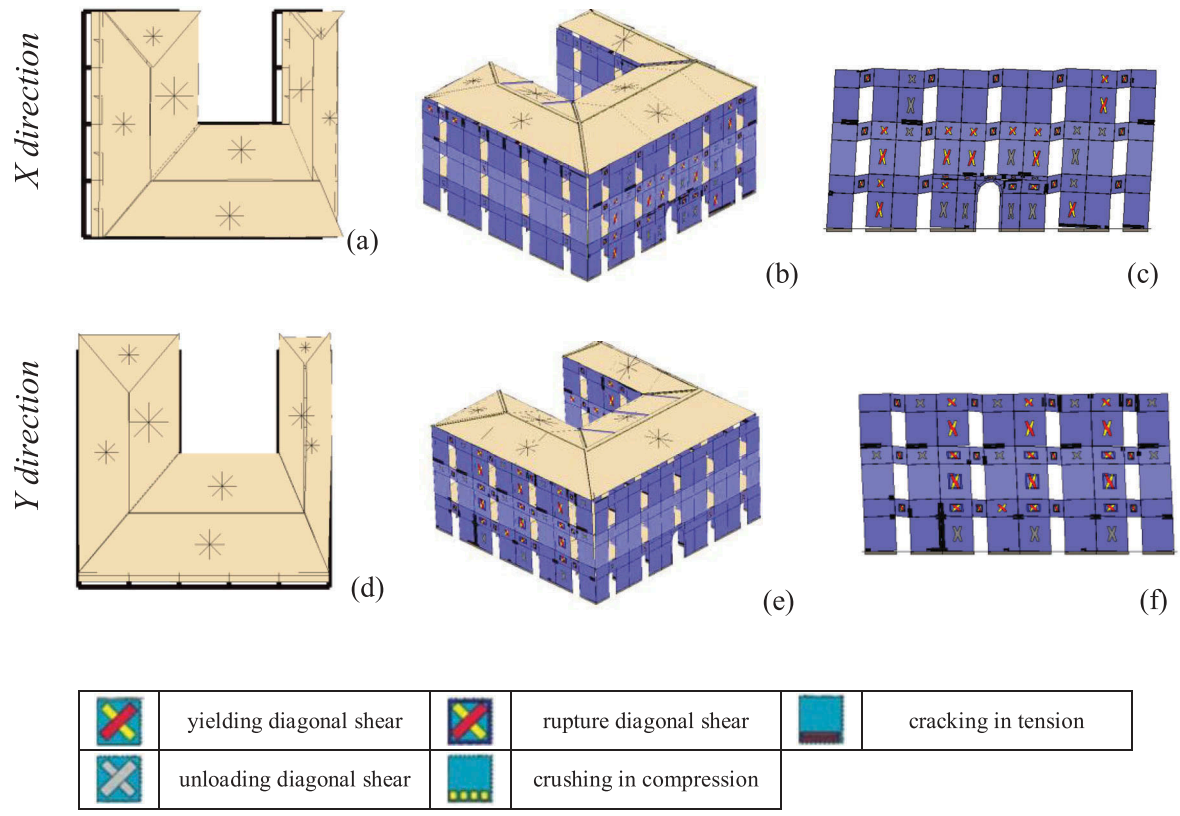

Figure 16. Collapse mechanisms of the **DA** model loaded in the *X* and *Y* directions: Plan view (a,d); 3D view (b,e); main facade (c,f).

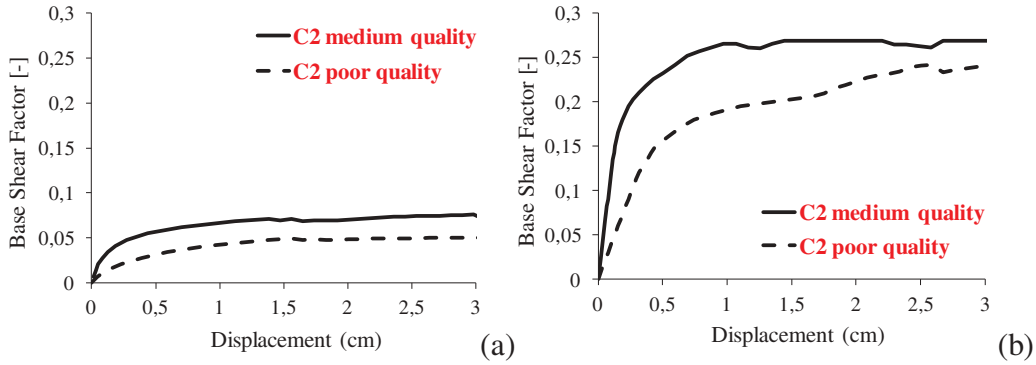

Figure 17. Influence of the quality of the masonry on the capacity curves of the typology **C2** in the *X* direction (a) and *Y* direction (b).

direction of the load. The spectral acceleration (S_{ay}) is evaluated as $V_b/(\Gamma m^* g)$, where m^* is the equivalent mass of the system associated to the *SDOF* system in the considered loading direction and g is the gravity acceleration. The main parameters of the equivalent *SDOF* systems are reported in the first part of Tables 4–5, respectively, for *X* and *Y* directions. In the tables, T^* is the equivalent period of the system, S_{ay} *and* δ_y are respectively the spectral acceleration and the displacements associated to the elastic . The ductility capacity of the system is evaluated ultimate limits, and $\mu = \delta_u/\delta_y$ is the capacity ductility of the system.

According to the code prescriptions, a limit value of 3 is considered for the ductility capacity of the system while the ductility demand is evaluated by means of the NTC 2018 design spectra. The admissible *PGA* at the ultimate limit state is evaluated by imposing that the ductility capacity is equal to the correspondent demand. The results of the seismic assessments for each model are reported in the last three columns of Tables 4–5 considering three different classes of soil (A, B, and C) corresponding respectively to a rigid, medium rigid and soft soil.

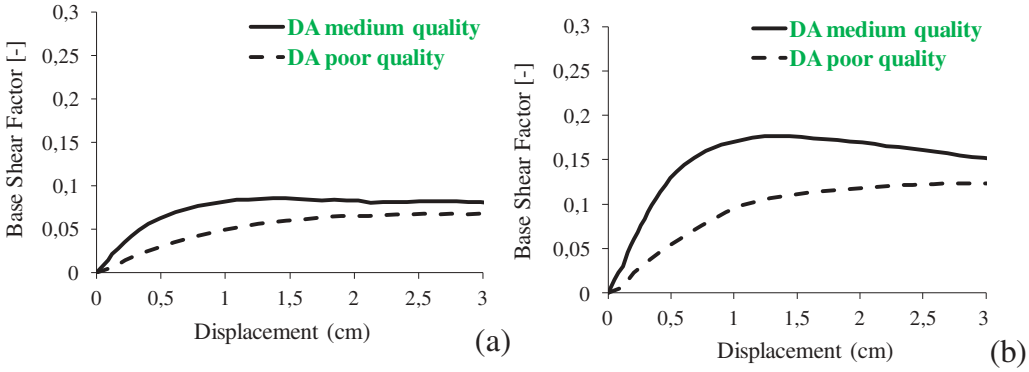

Figure 18. Influence of the masonry quality on the capacity curves of the typology **DA** in the *X* direction (a) and *Y* direction (b).

Table 4. Seismic assessment of the admissible PGA in *X* direction.

						PGA admissible (g)		
Typology	m* (Kg*10^3)	S_{ay} (g)	δ_y (mm)	Γ (-)	T* (sec)	Soil A	Soil B	Soil C
A1	175	0.14	0.7	1.00	0.082	0.23	0.20	0.18
A2	315	0.08	1.6	1.00	0.148	0.13	0.12	0.10
B1	551	0.04	2.5	1.53	0.412	0.07	0.06	0.05
B2	548	0.10	4.3	1.36	0.307	0.16	0.14	0.13
C2	1886	0.05	2.3	1.49	0.345	0.08	0.07	0.06
C3	2402	0.09	3.2	1.38	0.334	0.15	0.14	0.12
C4	3402	0.11	3.4	1.39	0.325	0.18	0.16	0.14
DA	6777	0.07	2.5	1.36	0.312	0.11	0.10	0.09
DC	7633	0.07	2.2	1.37	0.291	0.11	0.10	0.09

Table 5. Seismic assessment of the admissible PGA in *Y* direction.

						PGA admissible (g)		
Typology	m* (Kg*10^3)	S_{ay} (g)	δ_y (mm)	Γ (-)	T* (sec)	Soil A	Soil B	Soil C
A1	175	0.43	0.4	1.00	0.046	0.57	0.51	0.44
A2	315	0.46	0.7	1.00	0.058	0.56	0.50	0.44
B1	551	0.24	3.8	1.30	0.232	0.70	0.62	0.54
B2	548	0.33	0.4	1.22	0.069	0.40	0.36	0.31
C2	1886	0.27	2.1	1.30	0.165	0.40	0.35	0.31
C3	2402	0.24	2.0	1.30	0.167	0.36	0.32	0.28
C4	3402	0.22	2.1	1.44	0.177	0.38	0.33	0.29
DA	6777	0.14	4.3	1.34	0.278	0.59	0.52	0.46
DC	7633	0.16	3.1	1.33	0.245	0.52	0.46	0.41

The soil factor (S) and the corner periods (T_b, T_c), which characterize the response spectrum, are fixed coherently to the Italian code: namely, S = 1.00–1.13–1.29; T_b = 0.15–0.19–0.24 sec and T_c = 0.44–0.57–0.72 sec, respectively, for soil A, B, and C, while T_d = 2.74 sec is independent with respect to the soil characteristic.

The seismic safety factors are expressed, for each class of soil and load direction, as the ratio between the admissible *PGA* and the design *PGA* of 0.28 g that characterize the near collapse limit state for the site of interest. The latter has been determined considering the seismic risk map reported in the Italian code associated to soil A and probability of occurrence of 5% in 50 years. The graph of Figure 19 reports, for the three considered categories of soil, the seismic safety factors for each typology with respect to the weakest direction of each building.

In the loading direction *Y*, which is the direction with higher effective masonry area, all the considered typologies show a safety factor greater than 1, denoting a ductility capacity higher than the correspondent demand. However, in the *X* direction, where the openings are located, a strong decrease in the admissible ground acceleration is observed. This circumstance is coherent with the observations in occurrence of recent earthquakes, such as L'Aquila's earthquake in 2009 or the 2016 Centre Italy earthquakes, in which the historical masonry buildings exhibited different responses depending on the distributions of masonry panels and openings (Indirli et al. 2013; Carocci 2012; Cannizzaro et al. 2017).

In the *X* direction all the typologies, with the only exception of *A1* on soil A, have admissible *PGA* smaller than the design *PGA*. The smallest factors are observed for the typologies *B1* and *C2* while the highest safety coefficients are registered for the typologies *B2* and *C4*.

The class of soil strongly influences the seismic safety factors; average differences approximately of 15% and 25% are observed comparing, respectively, the assessments relative to soils B and C with the ones related to the soil A. The typologies *C* and *D* are more sensitive to the soil effects. Considering soils of class B, which are the most frequent in the old center of Catania, the average and minimum admissible *PGA*, among all the typologies, resulted, respectively, 45% and 20% of the expected in-situ *PGA*. The above results point out an unsafe scenario for the selected building typologies depending on the direction of the seismic input, even if the local out-of-plane mechanisms of the walls are avoided.

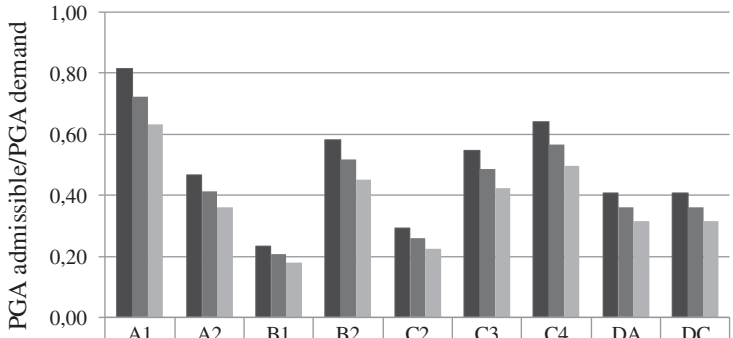

	A1	A2	B1	B2	C2	C3	C4	DA	DC
Soil A	0,82	0,47	0,23	0,58	0,29	0,55	0,64	0,41	0,41
Soil B	0,72	0,41	0,21	0,52	0,26	0,49	0,57	0,36	0,36
Soil C	0,63	0,36	0,18	0,45	0,23	0,42	0,50	0,32	0,32

Figure 19. Seismic vulnerability assessment of the isolated typologies with medium quality masonry.

5. The building aggregate

This section contains the results of the seismic analyses performed on an aggregate building obtained assembling the structural typologies investigated in Section 4. The two principal goals of the developed analyses are:

- to evaluate how the responses of the structural units change due to the interactions within the aggregate;
- to identify a general procedure for the seismic vulnerability assessment of building aggregate, as an extension of the N2-method employed in the case of isolated buildings.

In the following, an ideal aggregate realized assembling the nine structural typologies previously investigated, is considered. The geometrical layout of the structural units, within the aggregate, is chosen according to recurrent schemes present in the old centre of Catania. Following such scheme, the aggregate is characterized by an elongated shape with the largest structural typologies *DA* and *DC* located at the boundaries. The presence of the *in-line* typologies *C*, the mono-cellular *A* and the pluri-cellular *B* typologies characterizes the central part of the aggregate.

In the considered model the following simplifying hypotheses are assumed: (*i*) the walls belong to the same alignment, even referring to different typologies, are fully connected; (*ii*) two contiguous buildings share the common wall; and (*iii*) at each level the diaphragms are located at the same height for all the buildings. Furthermore, analogously to the case of isolated building models previously analyzed, the interaction between contiguous walls, as well as the out-of-plane masonry behavior, are neglected.

Figures 20a–b show a rendering 3D view of the considered aggregate and the computational model implemented in 3DMacro software. Figure 21 shows the first four modes of vibration of the aggregate together with the periods of vibration in the longitudinal (T_{ix}) and transversal (T_{iy}) directions (i = 1…4). In the same figure also the effective masses (M_{eff}) related to each mode are reported.

In the longitudinal direction all the reported periods are quite close to each other, in fact they range from 0.185 sec to 0.197 sec. The first two modes involve the central blocks composed by the *A*, *B*, and *C* building typologies and activate approximately 20% of the total mass of the aggregate. The third and fourth modes involve the external buildings and the percentage of the engaged mass is respectively 15% and 20%. Conversely, in the transversal direction the first two modes involve the external buildings and activate approximately 10% and 20% of the total mass. The other modes, associated to the central buildings, involve a small amount of mass.

Observing the modes of vibration of the aggregate shown in Figure 21, it is evident that the dynamic behavior of the aggregate is characterized by "local" modes of vibrations with very low levels of effective mass associated to each mode, ranging from 5–20% of the global mass of the aggregate.

In order to investigate the nonlinear behavior of the aggregate, pushover analyses in both directions have been performed considering mass proportional load distributions. This load distribution has been considered sufficiently representative of the inertia actions acting on the aggregate since the latter is composed by buildings of medium-low height. On the other hand, more in-depth numerical investigations would be required in order to apply push-over

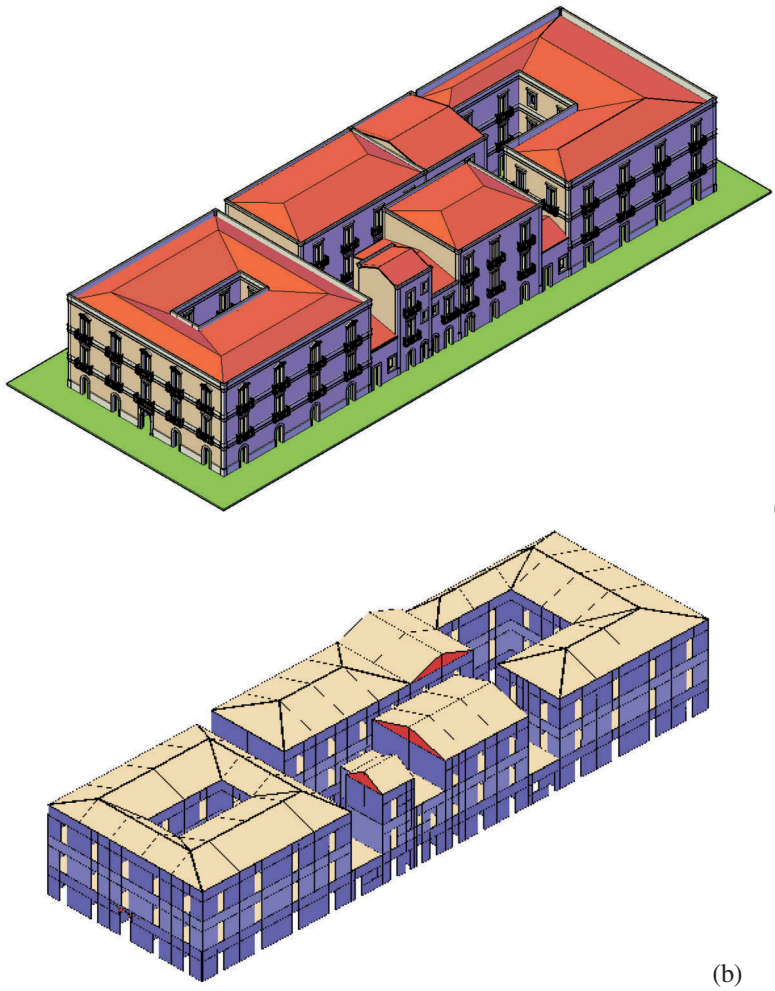

Figure 20. The investigate aggregate: rendering view (a) and computational 3DMacro model (b).

analyses considering a load distribution proportional to a combination of the fundamental vibration modes. These aspects are out of the scope of the article and will be managed in further research.

Nine control points, denoted as *P1–P9*, representative of each structural unit constituting the aggregate, are monitored during the push-over analyses. The location of each control point, shown in Figure 22, is chosen in order to properly describe the global response and collapse mechanism of each building unit of the aggregate. The control points from *P1–P8* coincide with the centres of gravity of the central span of the diaphragm at the top level of the represented buildings, while the point *P9*, relative to the *DA* typology, is located in the average value of the displacements at the top level of this building. Since each structural unit is monitored, the considered set of control points is able to investigate the torsion effects or potential local collapses, caused by the structural irregularity due to the diversity in the stiffness, strengths, and masses of the different building units. However, more control points could also be considered for each sub-element of the aggregate in order to investigate the possible torsion effects that can be activated within a single structural unit.

Figure 23 shows the capacity curves related to the monitored control points obtained performing the pushover analyses along the longitudinal (Figure 23a) and transversal (Figure 23b) directions of the aggregate considering masonry of medium quality. The maximum base shear coefficient resulted approximately to be 15% for both directions. In the transversal direction until C_b = 5% most curves show an approximately elastic behavior, after this limit some damage occurs causing a progressive degradation of the stiffness. Conversely, in the longitudinal direction the curves are nonlinear also for small intensities of the loads. The analyses are performed up to the peak global lateral strength when a conventional structural collapse is assumed. In order to investigate the post-peak behavior of the system a more sophisticated model, including the out-of-plane effects, should be employed. At the last

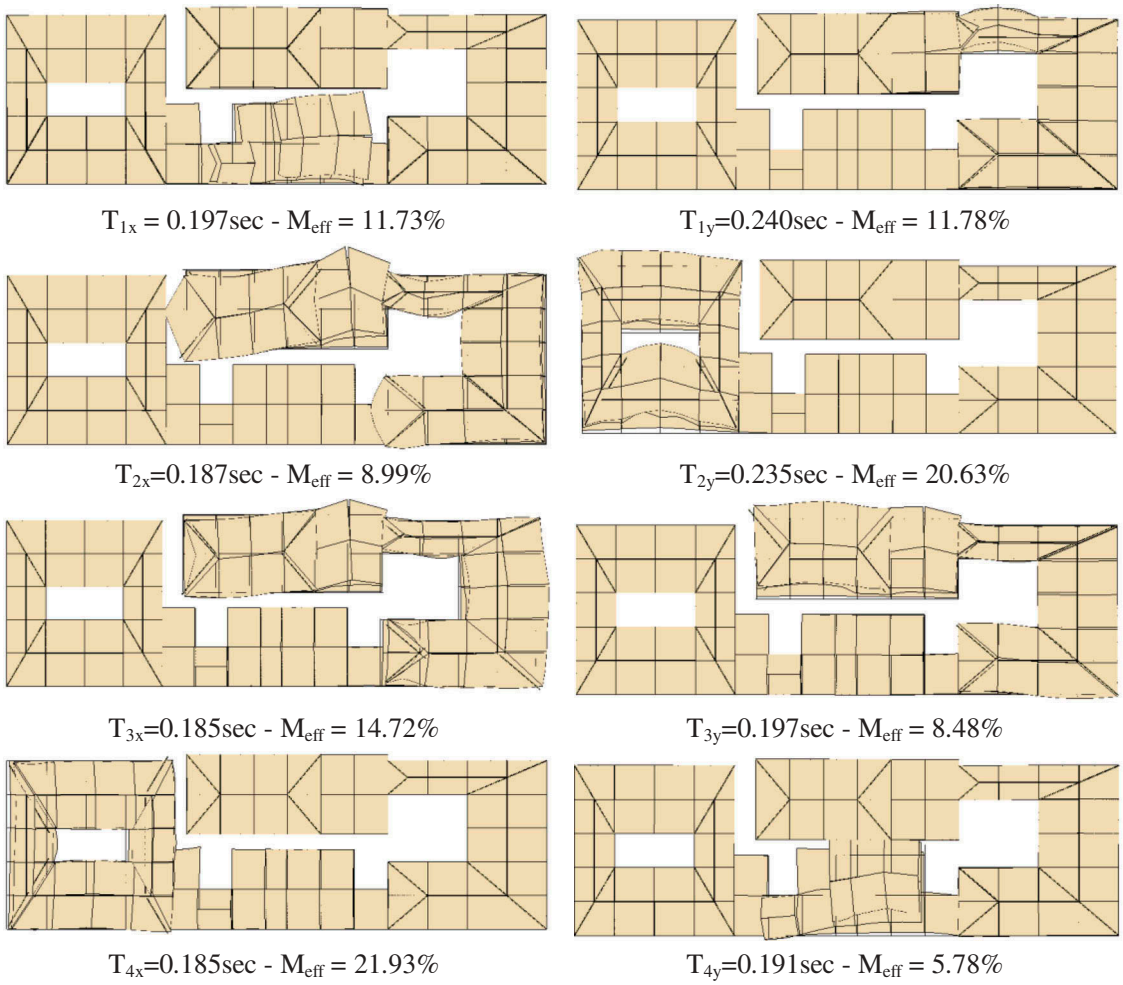

Figure 21. Fundamental modes of vibration and natural periods of the aggregate.

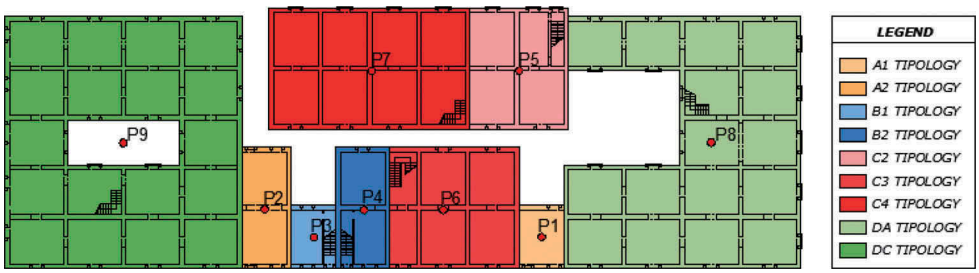

Figure 22. Typological plant of the aggregate with the control points considered in the analyses.

step of the analyses, different displacement capacities are observed in the structural units. In the longitudinal direction the maximum displacement of 1.90 cm is associated to the typology *B1* while the minimum displacement is associated to the typology *A2* with amplitude 0.60 cm. In the transversal direction, the maximum and minimum displacements are, respectively, 1.40 and 0.40 cm corresponding to the typology *DC* and *A2*, respectively. The in-plan irregularity of the aggregate is denoted by the large variability among the control point capacity curves in terms of stiffness, shape, and ultimate displacement, denoting a torsional motion of the aggregate. The deformed model at the last step of the analysis is reported in Figure 24 in both the investigated directions. An irregular damage distribution over the plane of the aggregate can be observed in the transversal direction where the internal units exhibit a horizontal shear deformation caused by their limited stiffness with respect to the external units. Also, the in-line units at the central part of the aggregate

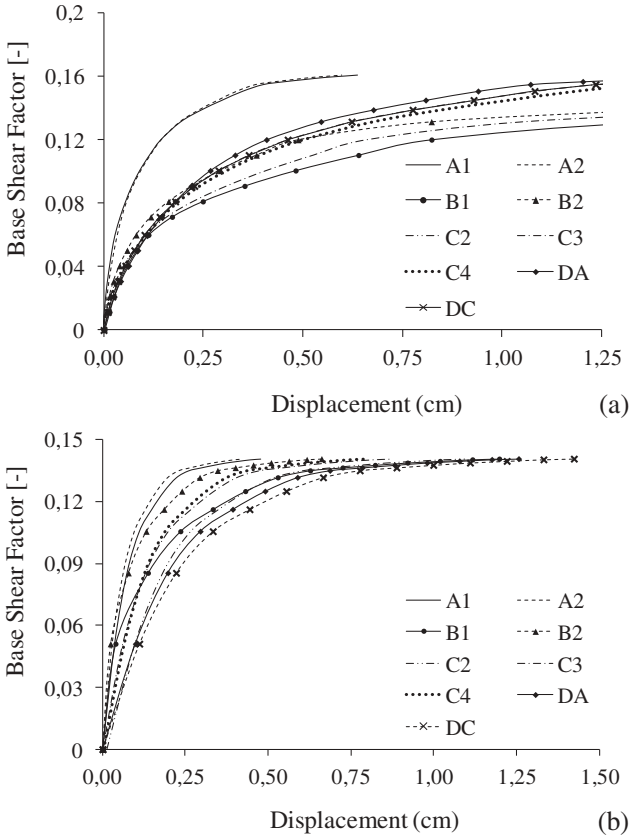

Figure 23. Capacity curves of the structural units within the aggregate (medium masonry quality) in longitudinal (a) and transversal (b) directions.

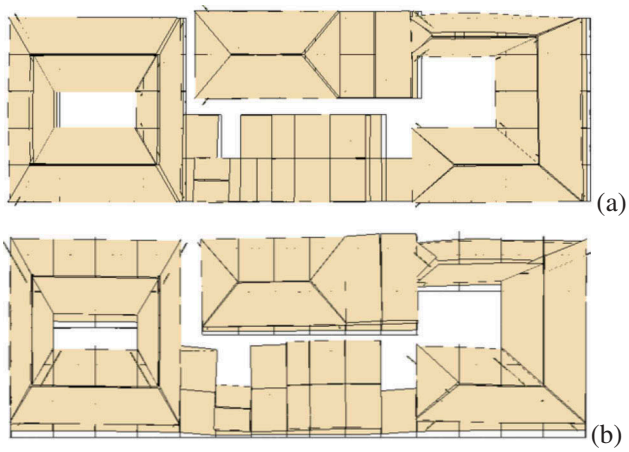

Figure 24. Global failure modes of the aggregate (medium masonry quality) in longitudinal (a) and transversal (b) directions.

show a torsional collapse for transversal loading actions.

Figure 25 reports the damage scenario in the main facades of the aggregate corresponding to the collapse state for the weak masonry model in both the investigated directions. It is possible to observe that the global damage path is characterized by the activation of combined diagonal shear failure and flexural (rocking) mechanisms.

A reduction of the presence of damage is observed in the lower buildings if compared to their condition when considered as isolated; this can be justified by the confinement effect provided by the contiguous taller structures. Conversely, the tallest structural units (terraced houses) show a wider distribution of damage, mainly concentrated at the panels of the top levels which are not contiguous with other buildings. The units with higher in-plane extension (patio houses) resulted severely damaged in both directions since they are located at the extremities of the aggregate. Hence, these buildings attract the torsion actions and don't benefit of a significant confinement effect from the adjacent structures.

In order to investigate the influence of the structural interactions within the aggregate on the sub-element responses, the capacity curves of each structural unit inserted in the aggregate are compared to the corresponding capacity curves (already reported in the previous section) obtained considering each typology as an isolated building. The results are reported in Figures 26–27 with reference respectively to the analysis in the longitudinal and transversal direction of the aggregate. The force parameter (λ) considered in the graphs represents the global external forces applied on the sub-element, normalized with respect to its seismic weight. Since the push-over analyses are performed considering a mass proportional loading distribution, λ coincides with the global base shear factor (C_b) of the aggregate. The global seismic weight (W) of the aggregate, computed analogously to the isolated buildings in section 4, resulted to be 169,000 kN.

It is worth noticing that, when the structural units are isolated, the load multiplier factor λ coincides with the base shear factor. On the contrary, when a structural unit is inserted in the aggregate, only a fraction of the all applied external forces is transferred through the base shear of that structural unit while the remaining part is transferred to the other units of the aggregate interacting through the continuous walls and diaphragms.

Considering the analysis in the longitudinal direction, the units in aggregate show higher strengths if compared to the correspondent isolated ones, denoting a positive confinement effect due to the mutual interaction with the other structures. At the same time, the stiffness of the structural units in the aggregate is generally increased because the aggregate is characterized by a lower global slenderness than that of the single structural units. As a consequence, the displacement capacities of the

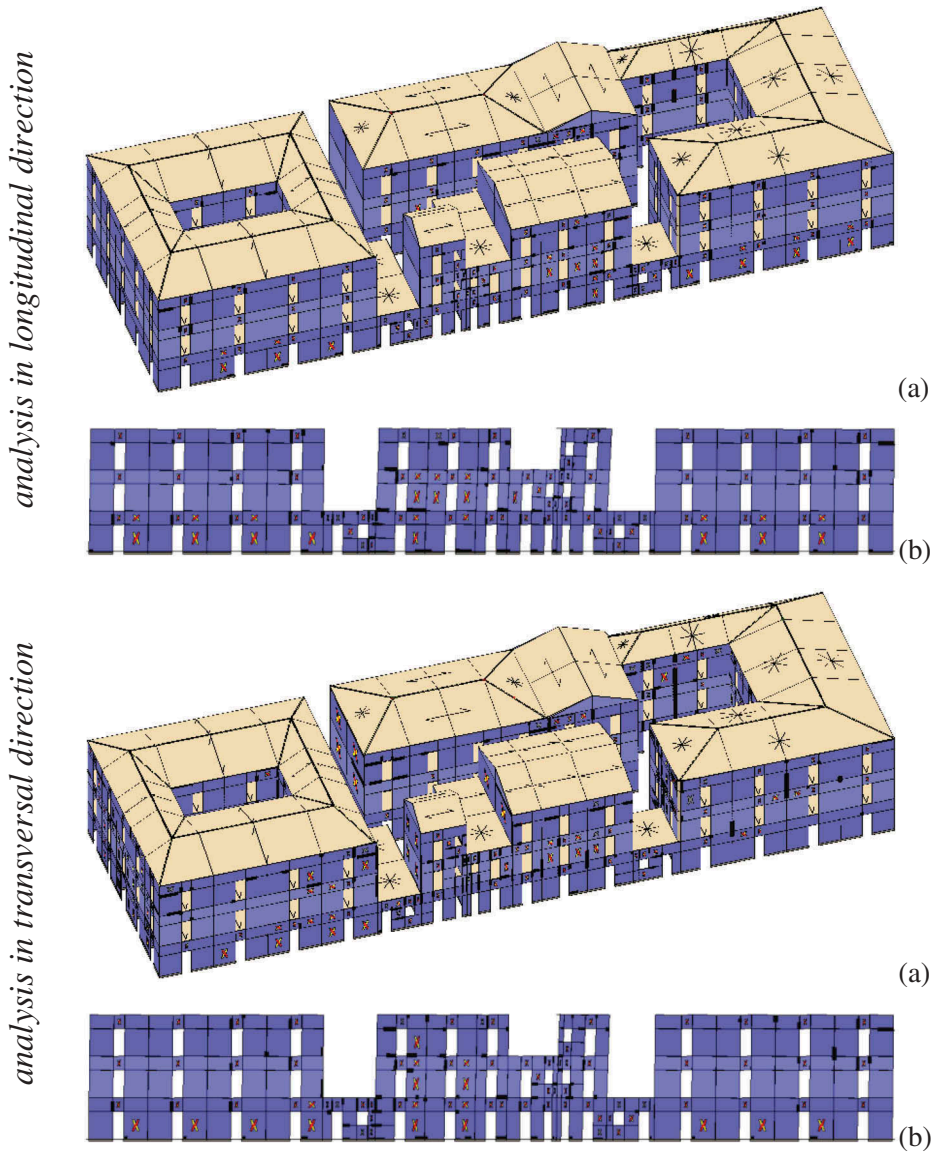

Figure 25. Plastic damage at the last step of analysis: 3D view of the aggregate (a) and main wall.

structural units within the aggregate are smaller compared to the correspondent capacities of the isolated buildings.

In the analysis in the transversal direction, the typologies with limited in-plane dimensions (*A* and *B*) show lower strength values with respect to the correspondent isolated structural units because they are constrained to follow the displacement of the external buildings that activate higher percentages of seismic actions. Conversely, the responses of the typologies *C* and *D* show smaller differences moving from the isolated to aggregate conditions. In this direction the initial lateral stiffness of the isolated units are comparable to the stiffness associated to the aggregate units highlighting a limited capacity of the aggregate to redistribute the seismic loadings and also the absence of any confinement effects.

The seismic assessment procedure, employed in the previous section to evaluate the seismic safety indices of the single structural units, is here extended to determine the seismic performance of each sub-element within the aggregate. The assessments are performed considering alternatively each control point representative of a single structural unit. An equivalent *SDOF* system is defined for each structural unit and load direction. The modal participation factors (Γ) and the effective masses (m^*) associated to each unit are evaluated considering its mass distribution and elastic deformation shape correspondent to the application of the mass-proportional load

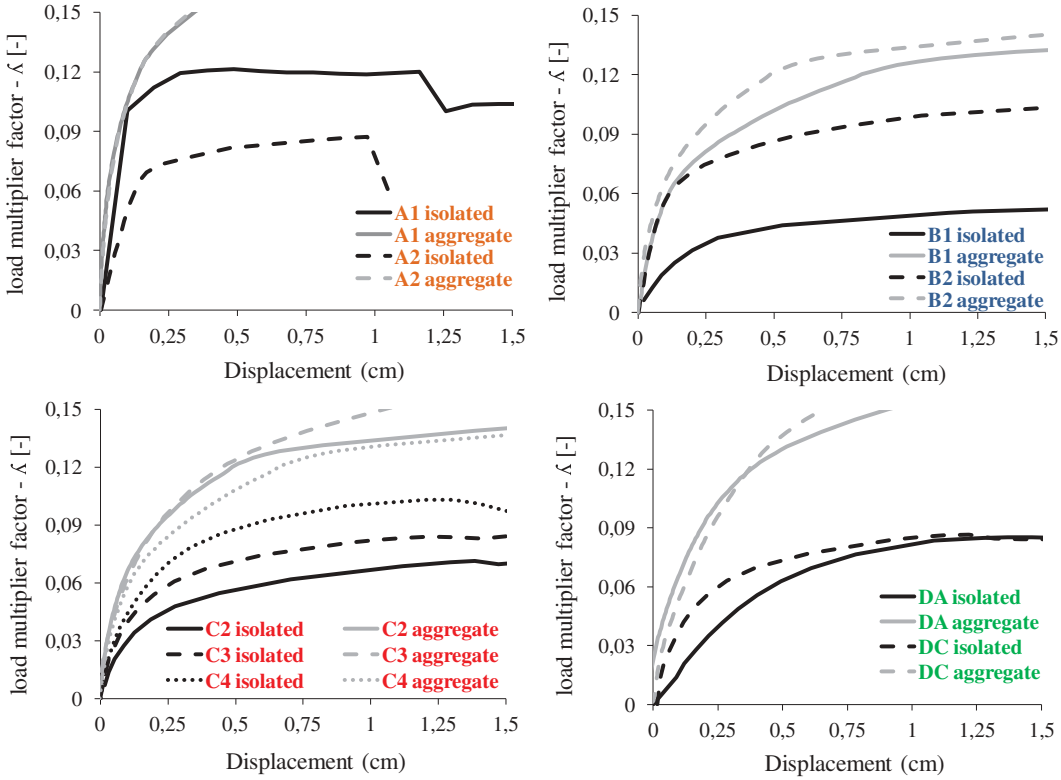

Figure 26. Comparison of the capacity curves of the aggregate and isolated structural typologies considering the analysis in the longitudinal direction.

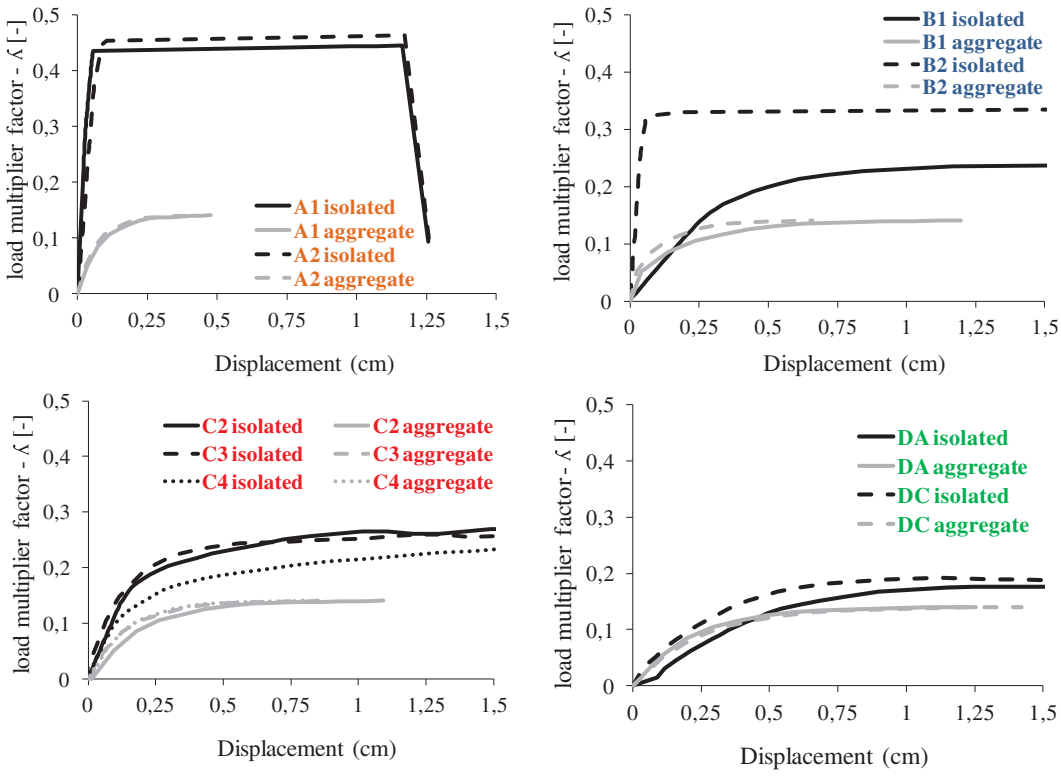

Figure 27. Comparison of the capacity curves of the aggregate and isolated structural typologies considering the analysis in the transversal direction of the aggregate.

Table 6. SDOF systems associated to the aggregate structural units (medium masonry quality).

	X Direction					*Y* Direction				
Typology	S_{ay} [g]	δ_y [mm]	Γ [-]	T* [sec]	μ capacity [-]	S_{ay} [g]	δ_y [mm]	Γ [-]	T* [sec]	μ capacity [-]
A1	0.144	1.06	1.00	0.17	2.96	0.139	0.81	1.00	0.17	2.40
A2	0.127	0.67	1.00	0.16	1.94	0.141	1.43	1.00	0.21	2.97
B1	0.137	2.15	1.32	0.27	4.53	0.140	1.47	1.28	0.24	6.37
B2	0.131	1.93	1.21	0.26	3.52	0.131	1.94	1.20	0.26	3.52
C2	0.127	1.92	1.26	0.24	2.56	0.141	1.90	1.20	0.23	4.52
C3	0.137	1.95	1.27	0.25	3.41	0.139	1.51	1.23	0.22	6.43
C4	0.137	1.72	1.27	0.28	3.67	0.140	1.40	1.21	0.23	6.15
DA	0.144	1.95	1.21	0.28	5.51	0.140	2.19	1.25	0.28	5.51
DC	0.137	5.24	1.26	0.28	3.02	0.139	2.07	1.23	0.25	5.51

distribution. The details of the equivalent SDF systems are reported in Table 6 with the same meaning of the symbols adopted in Tables 4–5.

Observing the results shown in Table 6, it is possible to conclude that the ductility capacities of all the *SDOF* systems, associated to the aggregate structural units, are sensibly smaller than the correspondent values for the isolated typologies. Furthermore, the *SDOF* periods (T^*) are increased for the small units and reduced for the typologies *C* and *D*. Both these aspects play a fundamental role in the evaluation of the admissible *PGA* applying the N2 method. Therefore, the seismic assessments of the single units, considered as isolated buildings, cannot be assumed to be representative of the effective safety level of the same buildings inserted within the aggregate.

The safety factors associated to each structural unit within the aggregate, for the three classes of soil, are reported in the graph of Figure 26 for both the longitudinal (Figure 26a) and transversal (Figure 26b) directions. Analogously to the vulnerability assessments of the single units, also in this case all the safety factors turn out to be smaller than 1 denoting a medium or high seismic vulnerability of the aggregate units. The safety factors in the transversal direction are sensibly smaller than those in the longitudinal direction with the only exception of the mono-cellular typology *A1*. Furthermore, in the transversal direction the safety factors are uniform in most of the units, ranging approximately from 20–40%. On the contrary, in the longitudinal direction a higher variability of the safety factors is observed (approximately from 20–60%): the three-story buildings show an average value of 45% and this decreases to 35% for the small buildings. The class of the soil, also in this case, influences sensibly the results, mainly in the case of tall buildings and longitudinal direction of loading. Comparing the safety factors of the aggregate and of the single isolated buildings, it is possible to observe an increase in the seismic vulnerability moving from

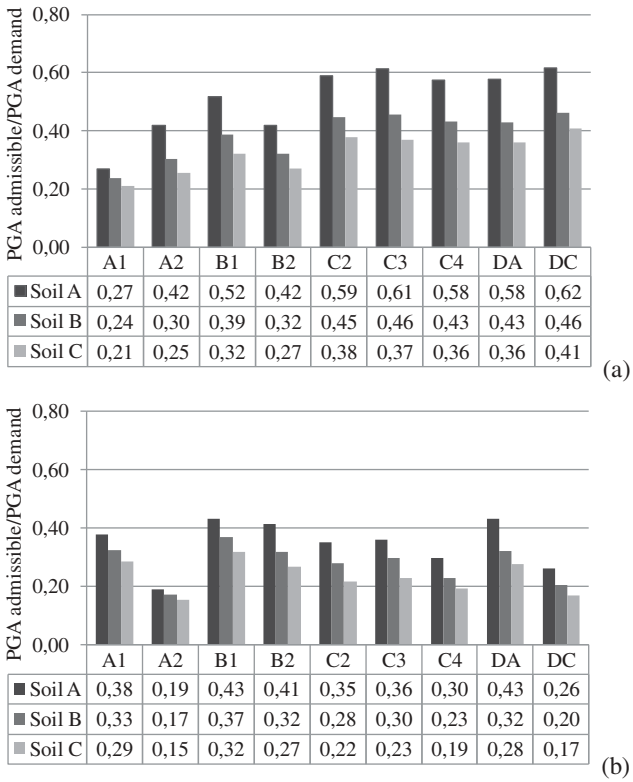

Figure 28. Seismic safety assessment of the sub-component of the aggregate along longitudinal (a) and transversal (b) directions considering a medium quality masonry.

the isolated (regular) typologies to the irregular disposition of the aggregate. The average reduction of the safety factor, considering all the buildings, is approximately equal to 25%, however some typologies are particularly influenced by the interaction with the other buildings. In particular, the highest reductions are registered for the typologies *A* and *C* (over 50%).

The results allow concluding that the small and central buildings are the most penalized by the aggregate disposition, if compared to the isolated condition. Conversely, the larger and lateral buildings are less affected by this interaction and their response is comparable with the one obtained for the single building.

6. Conclusions

This article summarizes the main results of a Catania University research project denomined "FIR 2014 ", focused on the Seismic vulnerability of historical masonry buildings built in Catania after the 1693 earthquake. A detailed analysis of the urban fabric of the historical centre of the city has been performed. The periodicity of the construction scheme has allowed recognizing a typical basic cell that has been analyzed individually and according to different geometrical arrangements representative of larger buildings or aggregates of buildings. Different construction typologies have been identified and numerically investigated through push-over analyses, employing a novel numerical approach based on a 2D macro-model able to simulate the nonlinear behavior of unreinforced masonry constructions with a limited computational effort. Seismic vulnerability assessments are performed following the N2 method and consistently to the Italian building code (NTC2018).

The examined structures turned out to be able to support from 30–50% of the current normative seismic demand, depending on the soil characteristics. Furthermore, a significant influence of the soil properties on the seismic safety has been observed providing a seismic safety reduction up to 25% depending on the investigated typologies and the loading direction.

A case study consisting in a typical building aggregate has been investigated aiming at evaluating how the interaction between the structural units influences the nonliner behavior and the seismic vulnerability. With respect to the seismic behavior of the isolated constructions, a general decrease in the seismic safety factors of the buildings within the aggregate is observed, obtaining an average value of 30%. This is due to the fact that the seismic interaction between the structural typologies, characterized by different stiffness, strength, and mass, produces torsional motions particularly for the smallest building units. The latter buildings, generally located in the central part of the aggregate, are subjected to significant relative displacements, imposed by the larger constructions located at the lateral areas of the aggregate.

Although the obtained results, concerning the investigated ideal building aggregate, highlight its high seismic vulnerability, an even higher vulnerability could be estimated in real aggregates due to the presence of irregular layouts, weak floor diaphragms, and out-of-plane failures.

The results obtained so far, although related to specific urban fabrics, could also be extended to other comparable areas and used for a better calibration of fast seismic assessment strategies.

Acknowledgments

The present research has been received funding from the MIUR (Italian Ministry for University and Research) within the project of the University of Catania FIR 2014, supervised by Professor Ivo Caliò, entitled "Seismic vulnerability of historical aggregate buildings: new methodologies for fast assessment and structural modelling."

Disclosure statement

No potential conflict of interest was reported by the authors.

ORCID

A. Greco http://orcid.org/0000-0003-2929-5044
G. Lombardo http://orcid.org/0000-0002-5226-4222
B. Pantò http://orcid.org/0000-0002-3340-228X

References

Anania, L., A. Badala, and M. Cuomo. 1995. *Mechanical characterization of historical mortars of Eastern Sicily. International Journal of British Masonry Society* 7:382–87.

Andreini, M., A. De Falco, L. Giresini, and M. Sassu. 2013a. Mechanical characterization of masonry walls with chaotic texture: Procedures and results of in-situ tests. *International Journal of Architectural Heritage* 8 (3):376–407. doi:10.1080/15583058.2013.826302.

Andreini, M., A. De Falco, L. Giresini, and M. Sassu. 2013b. Structural analysis and consolidation strategy of the historic mediceo aqueduct in pisa (Italy). *Applied Mechanics and Materials* 351 (352):1354–57. doi:10.4028/www.scientific.net/AMM.351-352.1354.

Andreini, M., I. Caliò, F. Cannizzaro, A. De Falco, L. Giresini, B. Pantò, and M. Sassu. 2014. Seismic assessment of the historical mixed masonry reinforced concrete government palace in La Spezia. Paper presented at the 9th International Conference on Structural Analysis of Historical Constructions, F. Peña & M. Chávez (eds.) Mexico City, October 14–17.

Barbera, S. 1992. *Tipi edilizi minori del centro storico di Catania*. Roma: Gangemi Editore.

Beolchi, C., G. Binda, L. Magenes, S. Cocina, L. Gambarotta, D. Liberatore, E. Lo Giudice, and S. Scuderi. 2000. *Tipologie edilizie in muratura del comune di Catania*. Roma: CNR - Gruppo Nazionale per la Difesa dai Terremoti.

Bertolesi, E., F. Fabbrocino, A. Formisano, E. Grande, and G. Milani. 2017. FRP-strengthening of curved masonry structures: Local bond behavior and global response. *Key Engineering Materials* 747:134–41. doi:10.4028/www.scientific.net/KEM.747.

Betti, M., G. Bartoli, and M. Orlando. 2010. Studio di valutazione su guasto strutturale di un palazzo rinascimentale italiano. *Strutture Ingegneristiche* 32:1801–13.

Betti, M., L. Galano, and A. Vignoli. 2014. Comparative analysis on the seismic behaviour of unreinforced masonry buildings with flexible diaphragms. *Engineering Structures* 61:195–208. doi:10.1016/j.engstruct.2013.12.038.

Binda, L. 2000. *Caratterizzazione delle murature in pietra e mattoni ai fini dell'individuazione di opportune tecniche di riparazione*. Roma: CNR - Gruppo Nazionale per la Difesa dai Terremoti.

Borri, A., M. Corradi, G. Castori, and A. De Maria. 2015. A method for the analysis and classification of historic masonry. *Bulletin of Earthquake Engineering* 13 (9):2647–65. doi:10.1007/s10518-015-9731-4.

Caddemi, S., I. Caliò, F. Cannizzaro, and B. Pantò. 2014. The seismic assessment of historical masonry structures. Paper presented at the 12th International Conference on Computational Structures Technology, Naples, Italy, September 2–5.

Caliò, I. 2011. La prova di taglio con martinetti piatti. Paper presented at the XIV ANIDIS. Conference on Seismic Engineering, Bari, Italy, September 18–22.

Caliò, I., and B. Pantò. 2014. A macro-element modelling approach of infilled frame structures. *Computers & Structures* 143:91–107. doi:10.1016/j.compstruc.2014.07.008.

Caliò, I., F. Cannizzaro, E. D'Amore, M. Marletta, and B. Pantò. 2008. A new discrete-element approach for the assessment of the seismic resistance of composite reinforced concrete-masonry buildings. Paper presented at the Seismic Engineering International Conference Commemorating the 1908 Messina and Reggio Calabria Earthquake, Reggio Calabria, Italy, July 8–11.

Caliò, I., M. Marletta, and B. Pantò. 2012. A new discrete element model for the evaluation of the seismic behaviour of unreinforced masonry buildings. *Engineering Structures* 40:327–38. doi:10.1016/j.engstruct.2012.02.039.

Cannizzaro, F., B. Pantò, M. Lepidi, S. Caddemi, and I. Caliò. 2017. Multi-directional seismic assessment of historical masonry buildings by means of macro-element modelling: Application to a building damaged during the L'Aquila earthquake (Italy). *Buildings* 7 (4):137–60. doi:10.3390/buildings7040106.

Carocci, C. F. 2012. Small centres damaged by 2009 L'Aquila earthquake: On site analyses of historical masonry aggregates. *Bulletin of Earthquake Engineering* 10:45–71. doi:10.1007/s10518-011-9284-0.

Casapulla, C., L. U. Argiento, and A. Maione. 2017a. Seismic analysis of an existing masonry building according to the multi-level approach of the Italian guidelines on cultural heritage. *Engineering Seismic* 34 (1):40–60.

Casapulla, C., L. U. Argiento, and A. Maione. 2017b. Seismic safety assessment of a masonry building according to Italian guidelines on cultural heritage: Simplified mechanical-based approach and pushover analysis. *Bulletin of Earthquake Engineering* 16 (7):2809–37. doi:10.1007/s10518-017-0281-9.

Cattari, S., S. Resemini, and S. Lagomarsino. 2008. Modelling of vaults as equivalent diaphragms in 3D seismic analysis of masonry buildings. In *Structural analysis of historic construction*, ed. D'sAyala, and Fodde, 517–24. London: Taylor & Francis Group.

Chácara, C., F. Cannizzaro, B. Pantò, I. Caliò, and P. B. Lourenço. 2018. Assessment of the dynamic response of unreinforced masonry structures using a macroelement modeling approach. *Earthquake Engineering & Structural Dynamics* 47 (12):2426–46.

Cicero, C., and G. Lombardo. 2015. *Establishment of an integrated Italy-Malta cross border system of civil protection, engineering aspects*. Rome, Italy: Roma Aracne Editrice.

D'Ambra, C., G. P. Lignola, A. Prota, E. Sacco, and F. Fabbrocino. 2018. Experimental performance of FRCM retrofit on out-of-plane behaviour of clay brick walls 2018. *Composites Part B:Engineering* 148:198–206. doi:10.1016/j.compositesb.2018.04.062.

Fagundes, C., R. Bento, and S. Cattari. 2017. On the seismic response of buildings in aggregate: Analysis of a typical masonry building from Azores. *Structures* 10:184–96. doi:10.1016/j.istruc.2016.09.010.

Fajfar, P., and P. Gaspersic. 1996. The N2 method for the seismic damage analysis of RC buildings. *Earthquake Engineering and Structural Dynamics* 25:31–46. doi:10.1002/(SICI)1096-9845(199601)25:1<31::AID-EQE534>3.0.CO;2-V.

Ferreira, T. M., R. Vicente, J. M. Da Silva, H. Varum, and A. Costa. 2013. Seismic vulnerability assessment of historical urban centres: Case study of the old city centre in Seixal, Portugal. *Bulletin of Earthquake Engineering* 11 (5):1753–73. doi:10.1007/s10518-013-9447-2.

Fiorentino, G., A. Forte, E. Pagano, F. Sabetta, C. Baggio, D. Lavorato, and S. Santini. 2018. Damage patterns in the town of amatrice after August 24th 2016 central Italy earthquakes. *Bulletin of Earthquake Engineering* 16 (3):1399–423. doi:10.1007/s10518-017-0254-z.

Formisano, A. 2017. Theoretical and numerical seismic analysis of masonry building aggregates: Case studies in San Pio Delle Camere, L'Aquila, Italy. *Journal of Earthquake Engineering* 21 (2):227–45. doi:10.1080/13632469.2016.1172376.

Fortunato, A., F. Fabbrocino, M. Angelillo, and F. Fraternali. 2017. Limit analysis of masonry structures with free discontinuities. *Meccanica* 53 (7):1793–802. doi:10.1007/s11012-017-0663-8.

Giresini, L., M. Sassu, C. Butenweg, V. Alecci, and M. De Stefano. 2017. Vault macro-element with equivalent trusses in global seismic analyses. *Earthquake and Structures* 12 (4):409–23. doi:10.12989/eas.2017.12.4.409.

Giuffre, A. 1993. *Sicurezza e conservazione dei centri storici: Il caso Ortigia*. Roma, Italy: La Terza. ISBN-13: 978-884204250

Gruppo Sismica s.r.l. 2012. *3DMacro 3D software di calcolo per la vulnerabilità sismica degli edifici in muratura. Manuale Teorico versione 1.11103101*. Catania: Gruppo Sismica s.r.l..

Indirli, M., L. A. S. Kouris, A. Formisano, R. P. Borg, and F. M. Mazzolani. 2013. Seismic damage assessment of unreinforced masonry structures after the Abruzzo 2009 earthquake: The case study of the historical centers of L'Aquila and Castelvecchio Subequo. *International Journal of Architectural Heritage* 7:536–78. doi:10.1080/15583058.2011.654050.

Lourenço, P. B., N. Mendes, L. F. Ramos, and D. V. Oliveira. 2011. Analysis of masonry structures without box behavior. *International Journal of Architectural Heritage* 5 (4–5):369–82. doi:10.1080/15583058.2010.528824.

Maio, R., R. Vicente, A. Formisano, and H. Varum. 2015. Seismic vulnerability of building aggregates through hybrid and indirect assessment techniques. *Bulletin of Earthquake Engineering* 13 (10):2995–3014. doi:10.1007/s10518-015-9747-9.

Maio, R., T. M. Ferreira, and R. Vicente. 2016. A critical discussion on the earthquake risk mitigation of urban cultural heritage assets. *International Journal of Disaster Risk Reduction* 27:239–47. doi:10.1016/j.ijdrr.2017.10.010.

Maio, R., T. M. Ferreira, R. Vicente, and J. Estêvão. 2016. Seismic vulnerability assessment of historical urban centres: Case study of the old city centre of Faro, Portugal. *Journal of Risk Research* 19 (5):551–80. doi:10.1080/13669877.2014.988285.

Mallardo, V., R. Malvezzi, E. Milani, and G. Milani. 2008. Seismic vulnerability of historical masonry buildings: A case study in Ferrara. *Engineering Structures* 30:2223–41. doi:10.1016/j.engstruct.2007.11.006.

Marques, R., G. Vasconcelos, and P. B. Lourenço. 2012. Pushover analysis of a modern aggregate of masonry buildings through macro-element modelling. Paper presented at the 15th International Brick and Block Masonry Conference, Santa Catarina, Brazil, June 3–6.

Marques, R., and P. B. Lourenço. 2011. Possibilities and comparison of structural component models for the seismic assessment of modern unreinforced masonry buildings. *Computers & Structures* 89:2079–91. doi:10.1016/j.compstruc.2011.05.021.

Marques, R., and P. B. Lourenço. 2014. Unreinforced and confined masonry buildings in seismic regions: Validation of macro-element models and cost analysis. *Engineering Structures* 64:52–67. doi:10.1016/j.engstruct.2014.01.014.

Marseglia, P. S., F. Micelli, M. Leone, and M. A. Aiello. 2014. Modelling of masonry vaults as equivalent diaphragms. *Key Engineering Materials* 628:185–90. doi:10.4028/www.scientific.net/KEM.628.185.

NTC 2018, Italian Ministry of Infrastructure, D.M. 2018. Aggiornamento delle «Norme tecniche per le costruzioni, GU Serie Generale n.42 del 20-02-2018 - Suppl. Ordinario n. 8.

NZSEE. 2015. *Assessment and improvement of the structural performance of buildings in earthquakes*. New Zealand Society for Earthquake Engineering (NZSEE) Project Technical Group. Rome, Italy: Italian Ministry of Infrastructure and Transport.

Pantò, B., E. Raka, F. Cannizzaro, G. Camata, S. Caddemi, E. Spacone, and I. Caliò. (2015). Numerical macro-modeling of unreinforced masonry structures: A critical appraisal. Paper presented at the Fifteenth International Conference on Civil, Structural and Environmental Engineering Computing, Prague, Czech Republic, September 1–4.

Pantò, B., F. Cannizzaro, I. Caliò, and P. B. Lourenço. 2017a. Numerical and experimental validation of a 3D macro-model for the in-plane and out-of-plane behavior of unreinforced masonry walls. *International Journal of Architectural Heritage* 11 (7):946–64.

Pantò, B., F. Cannizzaro, S. Caddemi, and Caliò. 2016. 3D macro-element modelling approach for seismic assessment of historical masonry churches. *Advances in Engineering Software* 97:40–59. doi:10.1016/j.advengsoft.2016.02.009.

Pantò, B., I. Caliò, and P. B. Lourenço. 2017b. Seismic safety evaluation of reinforced concrete masonry infilled frames using macro modelling approach. *Bulletin of Earthquake Engineering* 15:3871–95. doi:10.1007/s10518-017-0120-z.

Paquette, J., and M. Bruneau. 2006. Pseudo-dynamic testing of unreinforced masonry building with flexible diaphragm and comparison with existing procedures. *Construction and Building Materials* 20 (4):220–28. doi:10.1016/j.conbuildmat.2005.08.025.

Pujades, L. G., A. H. Barbat, R. González-Drigo, J. Avila, and S. Lagomarsino. 2012. Seismic performance of a block of buildings representative of the typical construction in the eixample district in Barcelona (Spain). *Bulletin of Earthquake Engineering* 10 (1):331–49. doi:10.1007/s10518-010-9207-5.

Ramaglia, G., G. P. Lignola, F. Fabbrocino, and A. Prota. 2018. Numerical investigation of masonry strengthened with composites. *Polymers* 10 (3):334. doi:10.3390/polym10030334.

Ramos, L. F., and P. B. Lourenço. 2004. Modeling and vulnerability of historical city centres in seismic areas: A case study in Lisbon. *Engineering Structures* 26 (9):1295–310. doi:10.1016/j.engstruct.2004.04.008.

Senaldi, I., G. Magenes, and A. Penna. 2010. Numerical investigations on the seismic response of masonry building aggregates. *Advanced Materials Research* 133:715–20. doi:10.4028/www.scientific.net/AMR.133-134.715.

Turnšek, V., and F. Čačovič. 1971. Some experimental results on the strength of brick masonry walls. Paper presented at the 2nd International Brick Masonry Conference. Proceedings:, Stoke-on-Trent, April 149–156.